21

AN OVERVIEW ON MOTOR VEHICLE AERODYNAMICS

The forces and moments the vehicle receives from the surrounding air depend more on the shape of the body than on the characteristics of the chassis. A detailed study of motor vehicle aerodynamics is thus beyond the scope of a book dealing with the automotive chassis.

However, aerodynamic forces and moments have a large influence on the longitudinal performance of the vehicle, its handling and even its comfort, so it is not possible to neglect them altogether.

Even if the goal of motor vehicle aerodynamics is often considered to be essentially the reduction of aerodynamic drag, the scope and the applications of aerodynamics in motor vehicle technology are much wider.

The following aspects are worth mentioning

- reduction of aerodynamic drag,
- reduction of the side force and the yaw moment, which have an important influence on stability and handling,
- reduction of aerodynamic noise, an important issue for acoustic comfort, and
- reduction of dirt deposited on the vehicle and above all on the windows and lights when driving on wet road, and in particular in mud or snow conditions. This aspect, important for safety, can be extended to the creation of spray wakes that can reduce visibility for other vehicles following or passing the vehicle under study.

G. Genta, L. Morello, *The Automotive Chassis, Volume 2: System Design*,
Mechanical Engineering Series,

The provisions taken to obtain these goals are often different and sometimes contradictory. A typical example is the trend toward more streamlined shapes that allow us to reduce aerodynamic drag, but at the same time have a negative effect on stability.

Another example is the mistaken assumption that a shape that reduces aerodynamic drag also has the effect of reducing aerodynamic noise. The former is mainly influenced by the shape of the rear part of the vehicle, while the latter is much influenced by the shape of the front and central part, primarily of the windshield strut (A-pillar). It is then possible that a change in shape aimed at reducing one of these effects may have no influence, or sometimes even a negative influence, on the other one.

At any rate, all aerodynamic effects increase sharply with speed, usually with the square of the speed, and are almost negligible in slow vehicles. Moreover, they are irrelevant in city driving.

Aerodynamic effects, on the contrary, become important at speeds higher than $60 \div 70$ km/h and dominate the scene above $120 \div 140$ km/h. Actually these figures must be considered only as indications, since the relative importance of aerodynamic effects and those linked with the mass of the vehicle depends on the ratio between the cross section area and the mass of the vehicle. At about $90 \div 100$ km/h, for instance, the aerodynamic forces acting on a large industrial vehicle are negligible when it travels at full load, while they become important if it is empty.

Modern motor vehicle aerodynamics is quite different from aeronautic aerodynamics, from which it derives, not only for its application fields but above all for its numerical and experimental instruments and methods. The shapes of the objects dealt with in aeronautics are dictated mostly by aerodynamics, and the aerodynamic fields contains few or no zones in which the flow separates from the body. On the contrary, the shape of motor vehicles is determined mostly by considerations like the possibility of locating the passengers and the luggage (or the payload in industrial vehicles), aesthetic considerations imposed by style, or the need of cooling the engine and other devices like brakes. The blunt shapes that result from these considerations cause large zones where the flow separates and a large wake and vortices result.

The presence of the ground and of rotating wheels has a large influence on the aerodynamic field and makes its study much more difficult than in the case of aeronautics, where the only interaction is that between the body and the surrounding air.

One of the few problems that are similar in aeronautical and motor vehicle aerodynamics is the study of devices like the wings of racing cars, but this is in any case a specialized field that has little to do with vehicle chassis design, and it will not be dealt with here in detail.

Traditionally, the study of aerodynamic actions on motor vehicles is primarily performed experimentally, and the wind tunnel is its main tool. The typical wind tunnel scenario is a sort of paradigm for interpreting aerodynamic phenomena, to the point that usually the body is thought to be stationary and

the air moving around it, instead of assuming that the body moves through stationary air.

However, while in aeronautics the two wiewpoints are coincident, in motor vehicle aerodynamics they would be so only if, in the wind tunnel, the ground moved together with the air instead of being stationary with respect to the vehicle. Strong practical complications are encountered when attempting to allow the ground to move with respect to the vehicle, and allowing the wheels to rotate. Usually, in wind tunnel testing, the ground does not move, but its motion is simulated in an approximate way.

Along with wind tunnel tests, it is possible to perform tests in actual conditions, with vehicles suitably instrumented to take measurements of aerodynamic forces while travelling on the road. Measurements of the pressure and the velocity of the air at different points are usually taken.

Recently powerful computers able to simulate the aerodynamic field numerically have became available. Numerical aerodynamic simulation is extremely demanding in terms of computational power and time, but it allows us to predict, with increasing accuracy, the aerodynamic characteristics of a vehicle before building a prototype or a full scale model (note that reduced scale models, often used in aeronautics, are seldom used in vehicular technology).

There is, however, a large difference between aeronautical and vehicular aerodynamics from this viewpoint as well. Nowadays, numerical aerodynamics is able to predict very accurately the aerodynamic properties of streamlined bodies, even if wind tunnel tests are needed to obtain an experimental confirmation. The possibility of performing extensive virtual experimentation on mathematical models greatly reduces the number of experimental tests to be performed.

Around blunt bodies, on the other hand, it is very difficult to simulate the aerodynamic field accurately, given their large detached zones and wake. Above all, it is difficult to compute where the streamlines separate from the body. The impact of numerical aerodynamics is much smaller in motor vehicle design than has been in aeronautics.

As said, the aim of this chapter is not to delve into details on vehicular aerodynamics, but only to introduce those aspects that influence the design of the chassis. While the study of the mechanisms that generate aerodynamic forces and moments influencing the longitudinal and handling performance of the vehicle will be dealt with in detail, those causing aerodynamic noise or the deposition of dirt on windows and lights will be overlooked. In particular, those unstationary phenomena, like the generation of vortices that are very important in aerodynamic noise, will not be studied.

21.1 AERODYNAMIC FORCES AND MOMENTS

In aeronautics, the aerodynamic force acting on the aircraft is usually decomposed in the direction of the axes of a reference frame $Gx''y''z''$, usually referred to as the *wind axes system*, centered in the mass center G, with the x''-axis

directed as the velocity of the vehicle with respect to air $-V_r$ and the z''-axis contained in the symmetry plane.

The components of the aerodynamic forces in the G$x''y''z''$ frame are referred to as drag D, side force S and lift L. The aerodynamic moment is usually decomposed along the vehicle-fixed axes Gxyz.

In the case of motor vehicles, both the aerodynamic force and moment are usually decomposed with reference to the frame xyz: The components of the aerodynamic force are referred to as longitudinal F_{x_a}, lateral F_{y_a} and normal F_{z_a} forces while those of the moment are the rolling M_{x_a}, pitching M_{y_a} and yawing M_{z_a} moments.

In the present text, aerodynamic forces will always be referred to frame xyz, which is centred in the centre of mass of the vehicle. However, in wind tunnel testing the exact position of the centre of mass is usually unknown and the forces are referred to a frame which is immediately identified.

Moreover, the position of the centre of mass of the vehicle depends also on the loading, while aerodynamic forces are often assumed to be independent of it, although a change of the load of the vehicle can affect its attitude on the road and hence the value of aerodynamic forces and moments.

The frame often used to express forces and moments for wind tunnel tests is a frame centred in a point on the symmetry plane and on the ground, located at mid-wheelbase, with the x'-axis lying on the ground in the plane of symmetry of the vehicle and the y'-axis lying also on the ground (Fig. 21.1). Since the resultant air velocity V_r lies in a horizontal plane, angle α is the aerodynamic angle of attack. From the definition of the x axis, it is a small angle and is often assumed to be equal to zero.

Remark 21.1 *From the definitions here used for the reference frames it follows that α is positive when the x-axis points downwards.*

The forces and moments expressed in the xyz frame can be computed from those expressed in the $x'y'z'$ frame (indicated with the symbols F'_x, F'_y, F'_z, M'_x, M'_y and M'_z) through the relationships

$$\begin{cases} F_x = F'_x \cos(\alpha) - F'_z \sin(\alpha) \\ F_y = F'_y \\ F_z = F'_x \sin(\alpha) + F'_z \cos(\alpha) \end{cases} \tag{21.1}$$

$$\begin{cases} M_x = M'_x + F_y h_G \\ M_y = M'_y - F_x h_G + F_z x'_G \\ M_z = M'_z - F_y x'_G \ . \end{cases} \tag{21.2}$$

Distance x'_G is the coordinate of the centre of mass with reference to the $x'y'z'$ frame and is positive if the centre of mass is forward of mid-wheelbase ($a < b$).

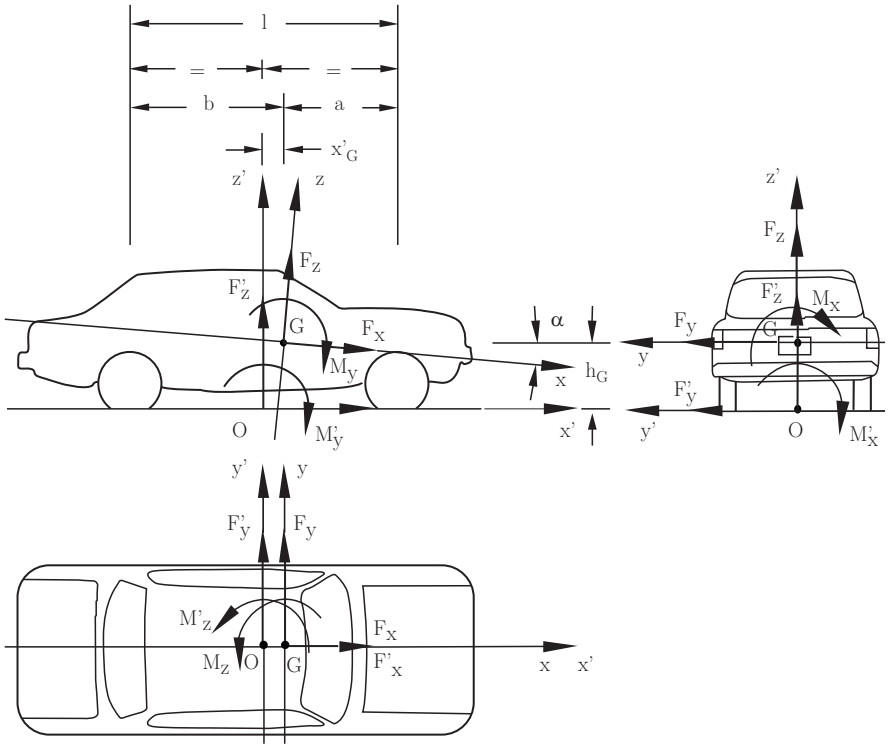

FIGURE 21.1. Reference frame often used to express aerodynamic forces in wind tunnel tests.

The air surrounding a road vehicle exerts on any point P of its surface a force per unit area

$$\vec{t} = \lim_{\Delta S \to 0} \frac{\Delta \vec{F}}{\Delta S} \,, \tag{21.3}$$

where ΔS and $\Delta \vec{F}$ are respectively the area of a small surface surrounding point P and the force acting on it.

The force per unit area $\vec{t}$ can be decomposed into a pressure force acting in a direction perpendicular to the surface

$$\vec{t}_n = p\vec{n} \,, \tag{21.4}$$

where $\vec{n}$ is a unit vector perpendicular to the surface and p is a scalar expressing the value of the pressure, and a tangential force $\vec{t}_t$ lying on the plane tangent to the surface. The latter is due to fluid viscosity.

These force distributions, once integrated on the entire surface, result in an aerodynamic force, which is usually applied to the centre of mass of the vehicle, and an aerodynamic moment. By decomposing the force and the moment in Gxyz frame, it follows:

$$\begin{cases} F_{x_a} = \displaystyle\int_S \vec{t_t} \times \vec{i} dS + \int_S \vec{t_n} \times \vec{i} dS \\ F_{y_a} = \displaystyle\int_S \vec{t_t} \times \vec{j} dS + \int_S \vec{t_n} \times \vec{j} dS \\ F_{z_a} = \displaystyle\int_S \vec{t_t} \times \vec{k} dS + \int_S \vec{t_n} \times \vec{k} dS \end{cases} \tag{21.5}$$

$$\begin{cases} M_{x_a} = -\displaystyle\int_S z\vec{t_t} \times \vec{j} dS + \int_S y\vec{t_t} \times \vec{k} dS - \int_S z\vec{t_n} \times \vec{j} dS + \int_S y\vec{t_n} \times \vec{k} dS \\ M_{y_a} = -\displaystyle\int_S x\vec{t_t} \times \vec{k} dS + \int_S z\vec{t_t} \times \vec{i} dS - \int_S x\vec{t_n} \times \vec{k} dS + \int_S z\vec{t_n} \times \vec{i} dS \\ M_{z_a} = -\displaystyle\int_S y\vec{t_t} \times \vec{i} dS + \int_S x\vec{t_t} \times \vec{j} dS - \int_S y\vec{t_n} \times \vec{i} dS + \int_S x\vec{t_n} \times \vec{j} dS \, . \end{cases} \tag{21.6}$$

At standstill, the only force exerted by air is the aerostatic force, acting in the vertical direction. It is equal to the weight of the displaced fluid. It reaches non-negligible values only for very light and large bodies and it is completely neglected in aerodynamics.

If air were an inviscid fluid, i.e. if its viscosity were nil, no tangential forces could act on the surface of the body; it can be demonstrated that in this case no force could be exchanged between the body and the fluid, apart from aerostatic forces, at any relative speed since the resultant of the pressure distribution always vanishes. This result, the work of D'Alembert, was formulated in 1744[1] and again in 1768[2]. It is since known as the D'Alembert Paradox.

In the case of a fluid with no viscosity, the pressure p and the velocity V can be linked to each other by the Bernoulli equation

$$p + \frac{1}{2}\rho V^2 = \text{constant} = p_0 + \frac{1}{2}\rho V_0^2 \, , \tag{21.7}$$

where p_0 and V_0 are the values of the ambient pressure and of the velocity far enough upstream from the body[3]. The term

$$p_d = \frac{1}{2}\rho V_0^2 \tag{21.8}$$

is the so-called dynamic pressure. The sum

$$p_{tot} = p_0 + p_d \tag{21.9}$$

is the total pressure.

---

[1] D'Alembert, *Traité de l'équilibre et du moment des fluides pour servir de suite un traité de dynamique*, 1774.

[2] D'Alembert, *Paradoxe proposé aux geometres sur la résistance des fluides*, 1768.

[3] Considering the actual case of the vehicle moving in still air, instead of the wind tunnel situation with air moving around a stationary object, V_0 is the velocity of the body relative to air $-V_r$.

TABLE 21.1. Pressure, temperature, density and kinematic viscosity of air at various altitudes, from the ICAO standard atmosphere. Only the part of the table related to altitudes of interest for road vehicles is reported.

z [m]	p [kPa]	T [K]	ρ [kg/m^3]	ν [m^2/s]
-500	107.486	291.25	1.2857	13.97×10^{-6}
0	101.325	288.16	1.2257	14.53×10^{-6}
500	95.458	284.75	1.1680	15.10×10^{-6}
1000	89.875	281.50	1.1123	15.71×10^{-6}
1500	84.546	278.25	1.0586	16.36×10^{-6}
2000	79.489	275.00	1.0070	17.05×10^{-6}
2500	74.656	271.75	0.9573	17.77×10^{-6}
3000	70.097	268.50	0.9095	18.53×10^{-6}

The values of the ambient pressure, together with those of the density, temperature, and kinematic viscosity at altitudes of interest in road vehicle technology, are reported in Table 21.1 from the ICAO standard atmosphere.

The density at temperatures and pressures different from p_a and T_a in standard conditions can be computed as

$$\rho = \rho_a \frac{p}{p_a} \frac{T_a}{T} \ , \tag{21.10}$$

where temperatures are absolute.

The dynamic pressure is extremely low, when compared to the ambient pressure: consider, for instance, a vehicle moving air at the temperature and pressure equal to those indicated in Table 21.1 at sea level, at a speed of 30 m/s (108 km/h). The pressure is about 101 kPa, while the dynamic pressure is 0,55 kPa, corresponding to 0,5% of pressure.

The variations of pressure due to velocity variations are thus quite small with respect to atmospheric pressure; however, such small pressure changes, acting on surfaces of some square meters, yield non-negligible, and sometimes large, aerodynamic forces.

Note that the Bernoulli equation, which holds along any streamline, was written without the gravitational term, the one linked with aerostatic forces. It states simply that the total energy is conserved along any streamline.

An example of the D'Alembert Paradox is shown in Fig. 21.2, where the cross section of a cylinder of infinite length, whose axis is perpendicular to the direction of the velocity V_r of the fluid, is represented. The streamlines open around the body and the local velocity of the fluid increases on its sides, leading to a decrease of pressure as described by the Bernoulli Equation. On the front of the body there is a point (actually in the case of the cylinder it is a line) which divides the part of the flow which goes "above" the body from that going "below" it. At this point, known as the stagnation point, the velocity of the fluid reduces to zero and the pressure reaches its maximum, equal to the total pressure.

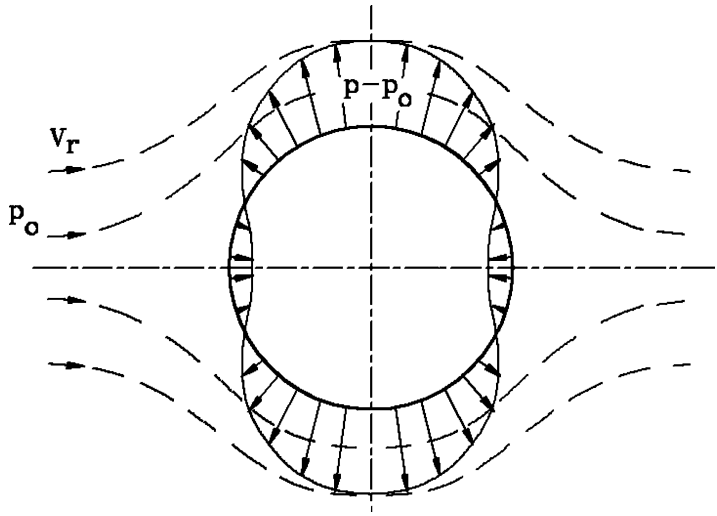

FIGURE 21.2. Streamlines and pressure distribution on a circular cylinder whose axis is perpendicular to the flow. This is a case of a fluid with no viscosity.

Since there is no viscosity, no energy is dissipated, and when the fluid slows down again, after reaching the maximum velocity at the point where the width of the body is maximum, the pressure is fully recovered: The pressure distribution is symmetrical and no net force is exchanged between the fluid and the body. This holds for any possible shape, provided that the viscosity is exactly nil.

No fluid actually has zero viscosity and the Paradox is not applicable to any real fluid. Viscosity has a twofold effect: It causes tangential forces creating so-called friction drag, and it modifies the pressure distribution, whose resultant is no longer equal to zero. The latter effect, which for fluids with low viscosity is generally more important than the former, generates the lift, the side force and the pressure drag. The direct effects of viscosity (i.e. the tangential forces) can usually be neglected, while the modifications of the aerodynamic field must be accounted for.

Owing to viscosity, the layer of fluid in immediate contact with the surface tends to adhere to it, i.e. its relative velocity vanishes, and the body is surrounded by a zone where there are strong velocity gradients. This zone is usually referred to as the "boundary layer" (Fig. 21.3) and all viscous effects are concentrated in it. The viscosity of the fluid outside the boundary layer is usually neglected and the Bernoulli equation can be used in this region.

Remark 21.2 *The thickness of the boundary layer increases as the fluid in it loses energy owing to viscosity and slows down. If the fluid outside the boundary layer increases its velocity, a negative pressure gradient along the separation line between the external flow and the boundary layer is created, and this decrease of pressure in a way boosts the flow within the boundary layer fighting its tendency*

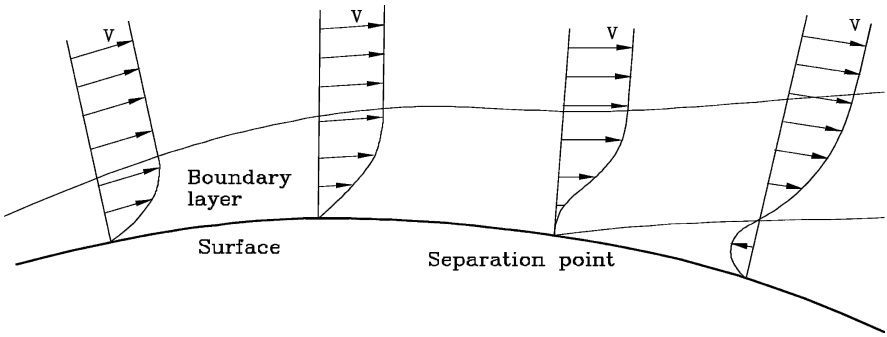

FIGURE 21.3. Boundary layer: Velocity distribution in direction perpendicular to the surface. The separation point is also represented.

to slow down. On the contrary, if the outer flow slows down, the pressure gradient is positive and the airflow in the boundary layer is hampered.

At any rate, at a certain point the flow in the boundary layer can stop and a zone of stagnant air can form in the vicinity of the body: The flow then separates from the surface, possibly starting the formation of a wake.

If the velocity distribution outside the boundary layer were known, the pressure distribution at the interface between the boundary layer and the external fluid could be computed. Provided that the boundary layer is very thin, and this is the case except where the flow is detached from the surface, the pressure on the surface of the body can be assumed to be equal to that occurring at the outer surface of the boundary layer, and then the aerodynamic forces and moments can be computed by integrating the pressure distribution. While this can be applied to computing the lift of streamlined objects, for blunt bodies, like the ones studied by road vehicle aerodynamics, and for drag, few results can be obtained along these lines.

To generalize the results obtained by experimental testing, performed mainly in wind tunnels, the aerodynamic force F and moment M are expressed as

$$F = \frac{1}{2}\rho {V_r}^2 S C_f \ , \qquad M = \frac{1}{2}\rho {V_r}^2 S l C_m \ , \tag{21.11}$$

where forces and moments are assumed to be proportional to the dynamic pressure of the free current

$$\frac{1}{2}\rho {V_r}^2 \ ,$$

to a reference surface S (in the expression of the moment a reference length l is also present) and to nondimensional coefficients C_f and C_m to be experimentally determined.

Such coefficients depend on the geometry and position of the body, and on two non-dimensional parameters, the Reynolds number

$$\mathcal{R}_e = \frac{Vl}{\nu} \ ,$$

and the Mach number

$$\mathcal{M}_a = \frac{V}{V_s} ,$$

where ν is the kinematic viscosity of the fluid (see Table 21.1) and V_s is the velocity of sound in the fluid.

The former is a parameter indicating the relative importance of the inertial and viscous effects in determining aerodynamic forces. If its value is low, the latter are of great importance, while if it is high aerodynamic forces are primarily due to the inertia of the fluid. In this case (for vehicles, if $\mathcal{R}_e > 3{,}000{,}000$), the dependence of the aerodynamic coefficients on the Reynolds number is very low and can be neglected. This is usually the case for road vehicles, at least for speeds in excess of $30 \div 40$ km/h.

If, on the contrary, the Reynolds number is low, aerodynamic forces and moments are essentially due to viscosity. In this case, their dependence on the velocity V should be linear rather than quadratic or, to use equations (21.11), the aerodynamic coefficients should be considered as dependent on the speed, increasing with decreasing speed.

The Mach number is the ratio between the airspeed and the speed of sound[4]. When its value is low, the fluid can be considered as incompressible; aerodynamic coefficients are then independent of speed. Approaching the speed of sound ($\mathcal{M}_a \sim 1$), the compressibility of the fluid can no longer be neglected and aerodynamic drag increases sharply. It is commonly thought that the Mach number is irrelevant in automotive aerodynamics, since the speeds road vehicles may reach, with the exception of some vehicles built to set speed records, lead to Mach numbers low enough to have practically no influence on aerodynamic coefficients. Actually this is true for streamlined bodies, for which the influence of Mach number is negligible for values up to $0,5 \div 0,6$ (speeds up to $600 \div 700$ km/h), while for blunt bodies fluid compressibility starts to play a role at a lower speed, even for Mach numbers slightly larger than 0,2 ($V = 70$ m/s $= 250$ km/h). As a consequence, the effects of the Mach number start to be felt at speeds that can be reached by racing cars. It is important to note that, owing to this effect of the Mach number, it is not possible to perform tests on reduced scale models by increasing the speed to increase the Reynolds number.

The reference surface S and length l are arbitrary, to the point that in some cases a surface not existing physically, like a power 2/3 of the displacement for airships, is used. These references simply express the dependence of aerodynamic forces on the square of the dimensions of the body and that of the moments on their cube. It is, however, clear that the numerical values of the coefficients depend on the choice of S and l, which must be clearly defined. In the case of road vehicles, the surface is that of the cross section, with some uncertainty about whether the frontal projected area or that of the maximum cross section has been used (Fig. 21.4).

---

[4]For air at sea level in standard conditions $V_s = 330$ m/s $= 1.225$ km/h.

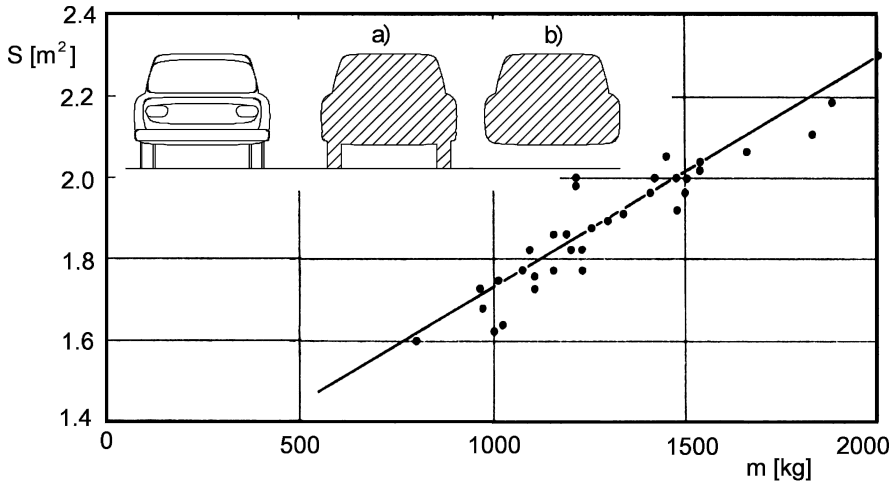

FIGURE 21.4. Area of the frontal projection of the vehicle as a function of its mass. a) Defnition of the frontal area; b) definition of the maximum cross-sectional area.

The mentioned SAE recommendation states that the frontal projected area, which should include the tires and the underbody parts, must be used. The reference surface is usually determined by using optical methods, by projecting a light beam on a screen, moving it to follow the outer shape of the vehicle. A simple but sometimes imprecise way of obtaining its value is

$$S = \psi b h \ , \tag{21.12}$$

where the value of coefficient ψ is about 0.81 and b and h are the width and the height of the vehicle. The area of the frontal area of various cars is reported as a function of their mass in Fig. 21.4. The points are well aligned on the straight line

$$S = 1.18 + 0.00056m \ , \tag{21.13}$$

where the surface is measured in m^2 and the mass in kg. The surface depends little on the mass, and its sensitivity can be measured by the derivative

$$\frac{dS}{dm} = 0.00056 \ . \tag{21.14}$$

The reference length l is usually the wheelbase, but in the expression of moment M_x the track t is often used.

The aerodynamic coefficients used in motor vehicle aerodynamics are those of the forces and moments decomposed along the vehicle axis system xyz: The longitudinal force coefficient C_x, the side force coefficient C_y, the normal force coefficient C_z, the rolling moment coefficient C_{M_x}, the pitching moment coefficient C_{M_y}, the yawing moment coefficient C_{M_z}.

21.2 AERODYNAMIC FIELD AROUND A VEHICLE

Consider a saloon car like the one sketched in Fig. 21.5. As usual in aerodynamics, assume a "wind tunnel" situation, i.e. consider the vehicle as stationary while the air flows around it.

The stream has a stagnation point at A, where the flow divides below and above the vehicle; in the vicinity of A the pressure takes the value p_{tot}. In the vicinity of B, the pressure takes values lower than the total pressure and even lower than the ambient pressure p_0, as the velocity increases, as shown in Fig. 21.6b, where the pressure distribution is reported in terms of pressure coefficient

$$c_p = \frac{p - p_0}{\frac{1}{2}\rho V_r^2} = 1 - \frac{V^2}{V_r^2} \,. \tag{21.15}$$

Note that the pressure coefficient is negative if the pressure is lower than the ambient pressure.

Remark 21.3 *As already stated, pressure variations $p - p_0$ are extremely small when compared to atmospheric pressure; however, their small value must not lead to the conclusion that aerodynamic forces are small: An overpressure equal to 0.5% of atmospheric pressure, like the one present at the stagnation point at 100 km/h acting on a surface of 1 m^2, yields a force of 500 N.*

After point C, located between B and the lower edge of the windshield, the flow detaches from the surface, to attach again at point D on the windshield.

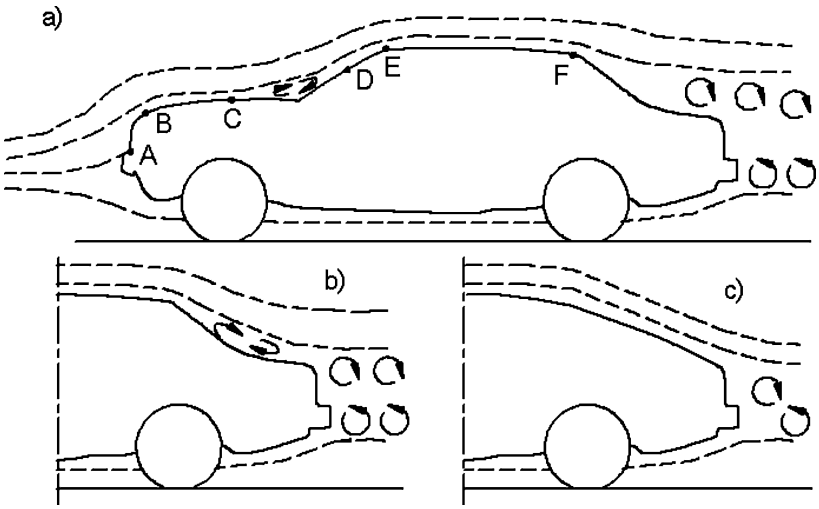

FIGURE 21.5. Streamlines about a passenger vehicle in the symmetry plane.

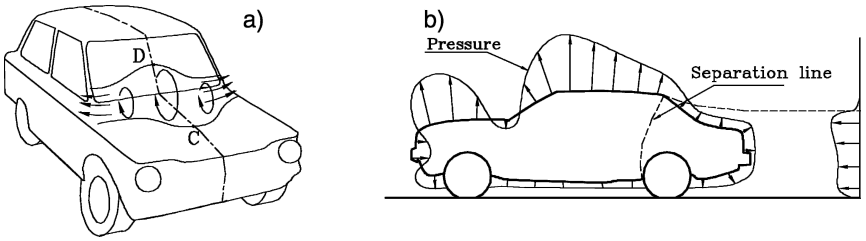

FIGURE 21.6. (a) Separation bubble on the windscreen of a car. (b) Pressure distribution on the symmetry plane of a saloon car and in the wake.

A separation bubble is formed between points C and D. The pressure in such a turbulent zone is fairly high, and it is reasonable to locate the intakes for ventilation of the passenger compartment there (Fig. 21.6). The separation bubble can be reduced by reducing the inclination of the windshield, which can be done only up to a limit since it may reduce visibility, or by increasing the transversal curvature of the windshield and of the hood. A curved windshield is effective in reducing drag but costs and also weighs more than a simple, flat one.

On the roof the pressure is again low, with a distribution that depends on its shape and curvature. At the end of the roof, the flow must slow down and the pressure should rise. In these conditions, the flow easily detaches and any surface irregularity can trigger the formation of the wake.

In Fig. 21.5a, the separation point has been located at the rear edge of the roof. There are cases in which the flow attaches again to the back of the trunk, giving way to a second separation bubble (Fig. 21.5b).

In the case of fastback cars with a sufficiently sloping back, the flow can remain attached up to the end of the body, giving way to a very small wake (Fig. 21.5c). The two situations are shown in the pictures of Fig. 21.7, obtained by visualizing the streamlines using smoke in a wind tunnel test.

The streamlines shown in Fig. 21.5 describe the situation occurring in the plane of symmetry. Outside this plane, the flow is no longer two-dimensional and tends to surround the vehicle at the sides as well.

This effect is generally beneficial and must be encouraged, as it tends to reduce all aerodynamic forces, giving a suitable curvature in the transverse direction to all surfaces. As already stated, point C can be moved further back by allowing the air to flow to the sides of the hood by lowering the fenders and giving them a curved shape; point D can be lowered by using a curved windshield. This results in a reduced separation bubble (Fig. 21.6).

The tridimensional flow on the back of the vehicle can cause vortices, as shown by tests on slanted blocks (Fig. 21.8). If angle α in the figure is lower than a critical value (about 62°), the flow separates abruptly, while for higher values the flow becomes strongly tri-dimensional and the streamlines which flow along the sides wind up in two large vortices while those flowing on the roof are deflected

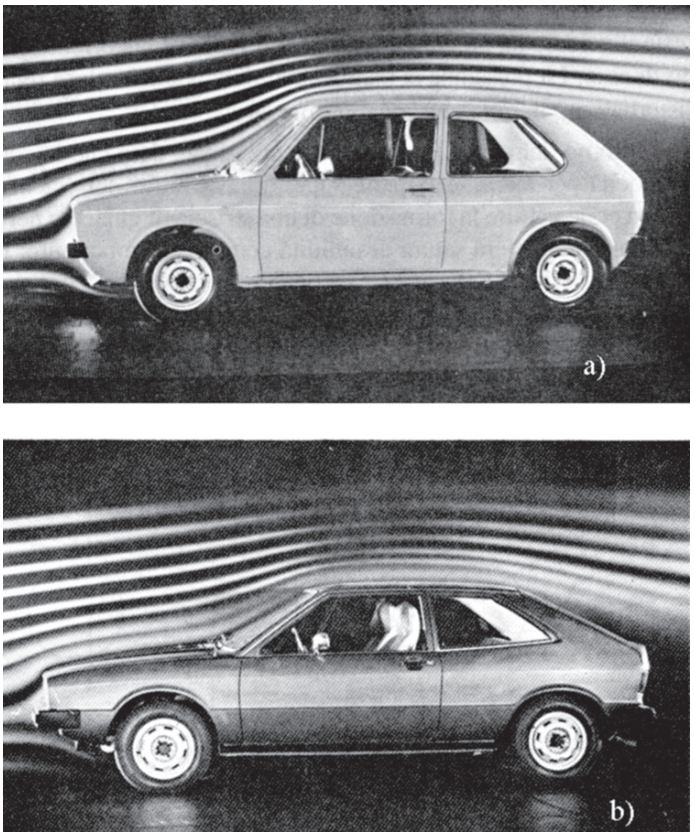

FIGURE 21.7. Streamlines in the symmetry plane about two fastback cars. In (a) the flow detaches at the end of the roof while in (b) it remains attached up to the end of the trunk.

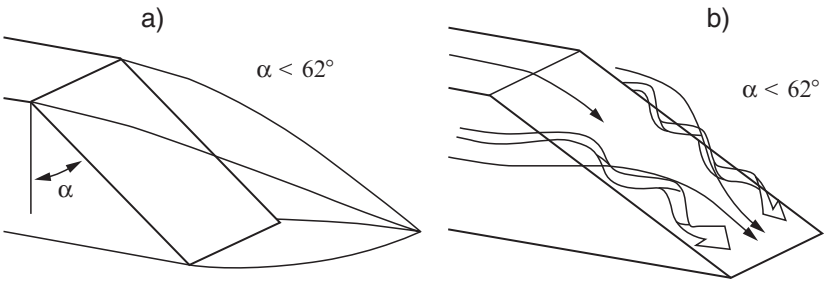

FIGURE 21.8. Flow on the back of slanted blocks.

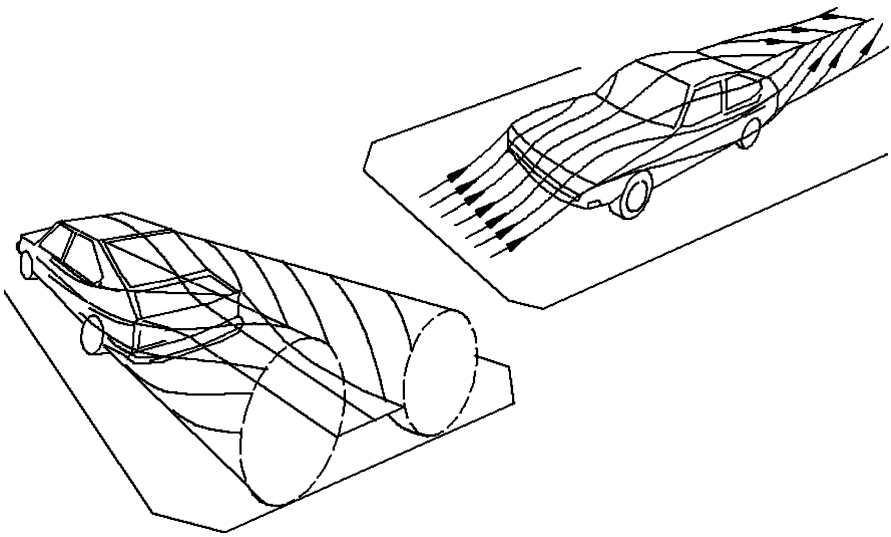

FIGURE 21.9. Qualitative pattern of the vortices behind a vehicle.

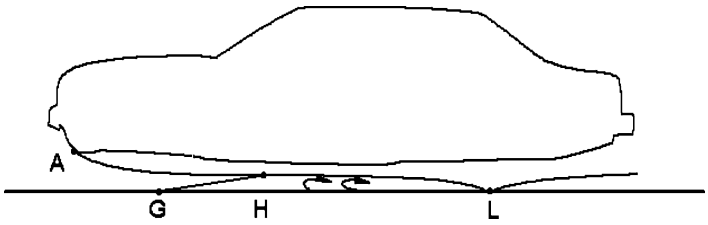

FIGURE 21.10. Flow below the vehicle. Boundary layer formation.

downwards and follow the tail of the vehicle. The flow in the symmetry plane, which is of the type shown in Fig. 21.9, is similar to that shown in Fig. 21.5c.

The wake is smaller, but this does not mean that the drag is lower: The pressure in the vortices is low, as is that on the centre of the tail since the flow is very fast in that zone: The overall pressure behind the vehicle can be even lower than that characterizing a large wake due to a small angle α.

The flow under the vehicle can be quite complicated and depends on many factors like the distance between vehicle and ground and the presence of a fairing under the body. Wind tunnel simulations can be misleading since in actual use the ground is stationary with respect to the air, at least if there is no wind, and not with respect to the vehicle, as occurs in wind tunnels.

In actual use, starting from the stagnation point A the boundary layer gradually thickens (Fig. 21.10). Outside the boundary layer, the velocity of the flow is different from that of the free stream, i.e., the flow is no longer at rest with respect to the ground, and from point G a second boundary layer appears on the ground as well.

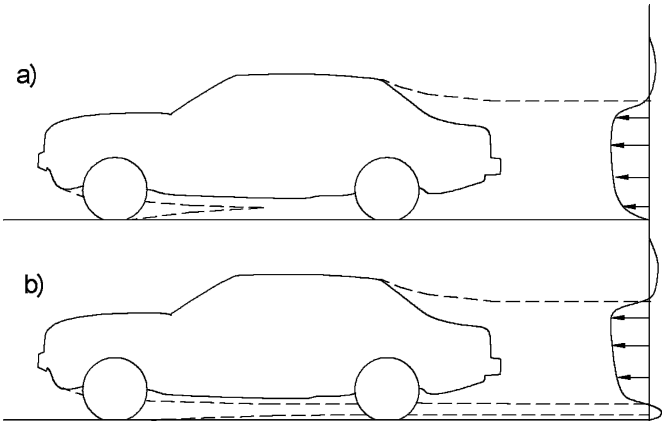

FIGURE 21.11. Effect of the shape of the bottom of the vehicle on the wake. (a) Bottom close to the ground and rough; (b) Streamlined bottom, at a greater distance from the ground.

Depending on the distance between the vehicle and the ground, the two boundary layers can meet in H or can remain separated. In the first case the flow is blocked and the air under the vehicle tends to move with it, giving way to another boundary layer starting from L. Between H and L a vortex may result. In the second case, the flow between the vehicle and the ground decreases aerodynamic lift, because of both the decreased size of the wake (Fig. 21.11) and the lower energy dissipation; if it is fast enough it causes a negative lift. The flow below the vehicle reduces the drag also, because the pressure in the wake is increased.

All improvements which facilitate the flow under the vehicle have these effects: Either the distance between vehicle and ground is increased or the bottom is given a curved shape, in the longitudinal or transverse direction, or the bottom is supplied with a smooth fairing covering the mechanical elements that are usually in the airflow. The last device may reduce the drag up to about $10 \div 15\%$, as shown in Fig. 21.12, but is seldom used in passenger cars as it is more difficult to reach the mechanical elements, making maintenance more costly.

These considerations cannot be generalized since any change of shape aimed at modifying the aerodynamic field at one point has an influence on the whole aerodynamic field, with effects that are difficult to predict.

Two effects can modify the airflow around the vehicle and make it more complicated: Wheel rotation and the presence of internal flows.

Consider a cylinder rotating and moving in directions consistent with those of a rolling wheel (Fig. 21.13a). It generates a drag and a lift (the Magnus effect)[5]

[5]A cylinder rotating with its axis perpendicular to the stream entrains, owing to viscosity, a certain quantity of air in rotation. On one side, the rotation velocity adds to the velocity of the stream; on the opposite side it subtracts. Where the velocity is higher the pressure is

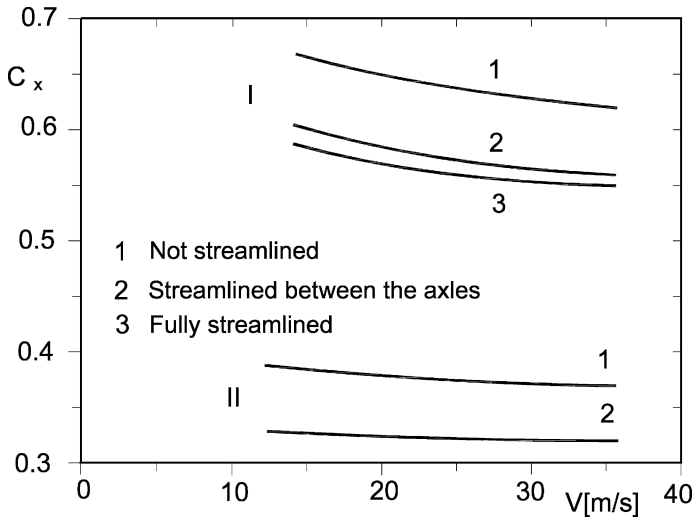

FIGURE 21.12. Effect of streamlining the bottom of the vehicle on the drag coefficient for two vehicles, I and II.

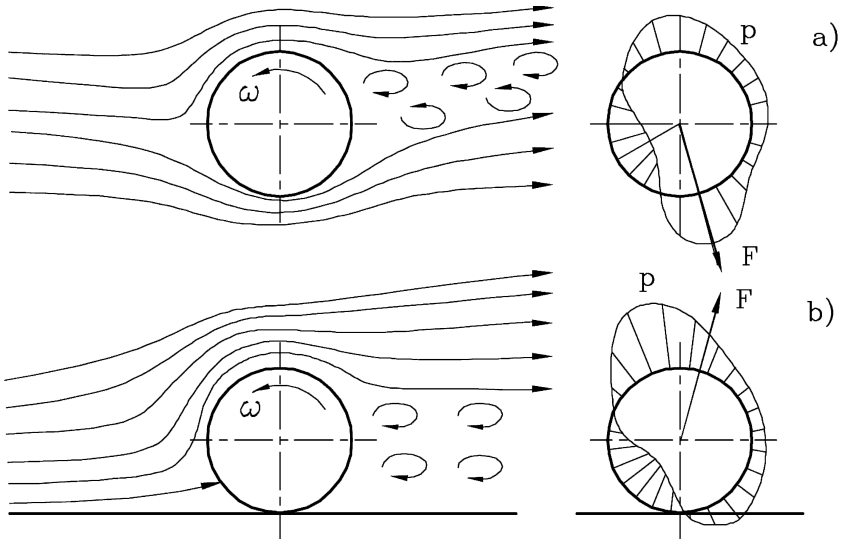

FIGURE 21.13. Streamlines, pressures and aerodynamic force acting on a wheel, modelled as a rotating cylinder, far from the ground (a) and in contact with it (b).

lower, with the effect on the other side. This pressure difference produces a force perpendicular to the axis of the cylinder and to the direction of motion. This effect is usually referred to as the Magnus effect.

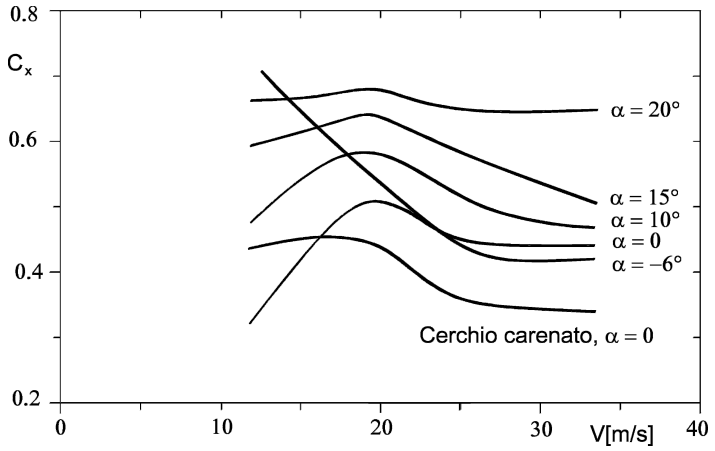

FIGURE 21.14. Drag coefficient of a rolling wheel. α is the sideslip angle.

which is directed downwards. If the wheel is in contact with the ground, however, the streamlines are completely changed by the presence of the latter and the lift becomes positive. The wake is larger and the drag coefficient increases; both the size of the first and the value of the second depend on the speed (Fig. 21.13b).

There is also an increase in drag owing to the larger wake, whose size depends also on the speed. The value of coefficient C_x of a rolling wheel, referred to the area of the cross section of the wheels, is plotted against the speed in Fig. 21.14.

As shown in the figure, the aerodynamic drag of a wheel increases if the wheel rolls with a sideslip angle measured with reference to the relative velocity of the air. In the case of the isolated wheel, this means that the drag depends on the sideslip angle of the wheel, while in normal conditions the flow is not parallel to the symmetry plane of the wheel even if the sideslip of the latter is zero, since the flow under the vehicle is deflected sideways. This effect is, in general, larger for front wheels and causes an increase in their aerodynamic drag. Streamlining the wheels in such a way to reduce drag has the limitation that the shape of the hubs must be studied so as to guarantee an appropriate cooling of the brakes.

Since the drag coefficient of a rolling wheel exposed to the airflow is about 0.45, it would seem that there is an advantage in inserting the wheels within the body only if the drag coefficient of the vehicle is lower than that value. However, all vehicles except formula racing cars have covered wheels for reasons different from drag reduction. Uncovered wheels are present in racing cars only when rules explicitly dictate. In Formula 1 racers, up to 45% of the aerodynamic drag can be ascribed to the wheels.

A sketch of the streamlines around a partially covered wheel is shown in Fig. 21.15, together with a plot of coefficients C_x and C_z versus the ratio h/D between the amount of wheel covered and its diameter. The curves are experimental and, particularly as related to C_z not very reliable owing to the method used to simulate the presence of the ground, but the results are at least qualitatively significant.

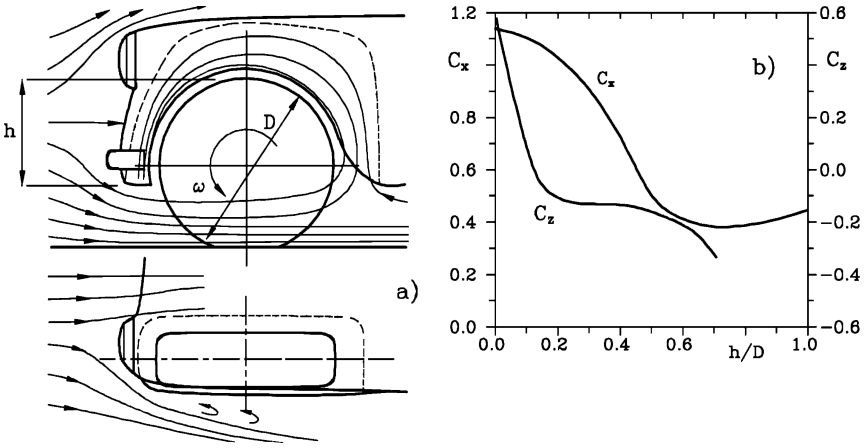

FIGURE 21.15. (a) Flow in the cavity around a covered wheel. (b) Aerodynamic coefficients of the wheel as functions of ratio h/D.

The advantage of covering the wheel, without exceeding a value $h/D = 0.5 \div 0.7$, is clear. The values of C_x are generally very high, particularly if compared with those of an isolated wheel, and the increase in drag when the wheel is largely covered can be explained by viscous effects within the fender.

Another reason for the deviation of the aerodynamic field from that shown in Fig. 21.5 is the presence of internal flows. There are usually two separate flows inside the vehicle: A cooling flow in the engine compartment, and a flow in the passenger compartment; other internal flows of lesser importance are those aimed at cooling mechanical devices such as brakes or the oil radiator, if it is located separately from the main radiator, etc.

The second flow is of lesser importance: If the intake is set at the base of the windshield and the outlet is in a zone in the wake, the result can be that of reducing the drag slightly, as this configuration reduces the pressure in the separation bubble and increases that in the wake.

A larger amount of air is needed for engine cooling. A good solution would be to use a radiator of the type common in water-cooled aircraft piston engines, in which a diffuser slows down the flow that is driven through the heat exchanger before being accelerated again in a converging duct (Fig. 21.16a). In motor vehicles, a fan allowing cooling with the vehicle stationary must also be provided. The diffuser should be long enough to allow the flow to be slowed down without separation (a slope of about 7° has been found to be a practical maximum) and the fan should operate only at speeds lower than those for which the system has been designed.

In practice, this solution cannot be used, at least on normal vehicles: A system of this type would be too long to be accommodated in the hood; instead there is a short diffuser whose opening is too large to allow a good attached flow, followed by a radiator. The flow then goes directly into the engine compartment

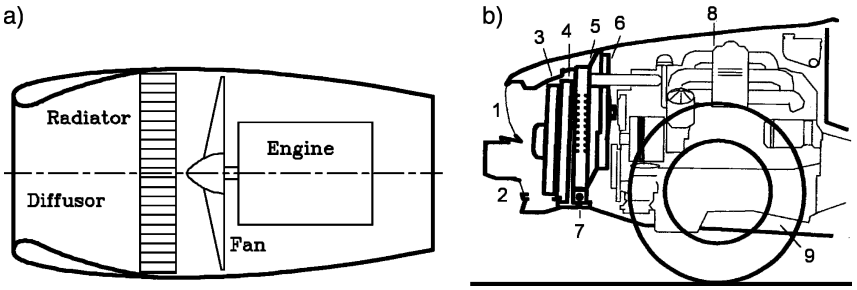

FIGURE 21.16. (a) Ideal radiator. (b) Actual layout of the cooling system in the engine compartment. 1) upper air intake; 2) lower air intake; 3) auxiliary fan; 4) air conditioning radiator; 5) radiator; 6) fan; 7) oil radiator; 8) engine; 9) air outlet.

without further guidance. The internal flow then mixes with the flow passing under the vehicle in a very disordered way. This situation is sketched in Fig. 21.16b. The complexities needed for obtaining a well guided flow, separated from the external flow, are considered not worth the added cost and weight and the difficulties they would add to maintenance operations in the engine compartment.

The presence of the internal flow in the engine compartment has a non-negligible influence on drag, lift, pitching moment and, although to a lesser extent, yawing moment. It can account for about 13% to 20% of the total drag; the increase in lift (generally positive, i.e. upwards) is even larger. The effect on moments is to move forward both lift (pitching moment) and side force (yawing moment). As will be seen later, both effects are detrimental to the overall behavior of the vehicle.

Aerodynamic testing should always be performed on models which reproduce the inside of the engine compartment as well or, better, on the actual vehicle, with open air intakes. Since the engine temperature affects the internal flow, aerodynamic testing should be done with the engine at running temperature.

21.3 AERODYNAMIC DRAG

As already stated, aerodynamic drag is the component of the aerodynamic force acting in the direction of the relative velocity, and thus the force that opposes the motion of the body in the fluid. If the relative velocity is confined to the symmetry plane (motion with no sideslip, and no lateral wind) the difference between drag and force F_x is quite small; this is due to the fact that the angle between the x-axis and the plane of the road is small, and that the aerodynamic efficiency, that is, the ratio between lift and drag, of motor vehicles is very low, if not equal to zero. In the case of road vehicles, the two are sometimes confused and force F_x is referred to as drag.

Remark 21.4 *In many cases, drag is considered positive when directed backwards, which is inconsistent with the general conventions on forces.*

Aerodynamic drag can be considered as the sum of three terms: Friction drag, shape drag and induced drag. Coefficient C_x can be similarly considered as the sum of the three corresponding terms

$$C_x = C_{x_a} + C_{x_f} + C_{x_i} \ . \tag{21.16}$$

While in aeronautics this subdivision is practically important, since the three terms can be computed separately in the various flight conditions, in the case of motor vehicles they cannot actually be separated. To consider them one by one is important only insofar it allows one to understand how the various components of the drag originate.

21.3.1 Friction drag

Friction drag is the resultant of the tangential forces acting on the surface

$$\int_S \vec{t}_t \times \vec{i} dS \ .$$

Since it is practically impossible to measure the friction drag on a body with complex geometry, reference is usually made to flat plates, where the only drag present is friction drag. Friction drag coefficient C_f, referring to the "wet" surface, i.e. to the surface exposed to the fluid, is plotted versus the Reynolds number, computed with reference to the length of the plate, as shown in Fig. 21.17.

The two straight lines (in the logarithmic plot) refer to a laminar and a turbulent flow in the boundary layer. They are approximated by the empirical relationships

$$C_f = \frac{1.328}{\sqrt{\mathcal{R}_e}} \ , \text{ or } C_f = \frac{0.074}{\sqrt[5]{\mathcal{R}_e}} \ , \tag{21.17}$$

respectively.

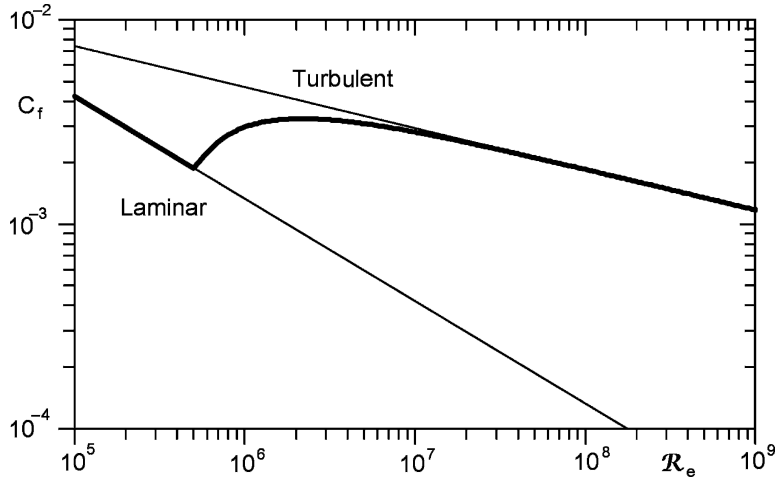

FIGURE 21.17. The friction coefficient referred to the wet surface versus the Reynolds number.

The flow is laminar if it is free from vorticity and there is no mixing between adjacent streamlines. The vortices which are present in a turbulent boundary layer are very small, but cause a mixing and a strong energy transfer within the layer. If the fluid is free from vorticity when it enters into contact with the plate, a laminar flow is maintained up to values of the Reynolds number of about 500,000, provided that surface irregularities do not trigger turbulence. If the Reynolds number is higher, at least a part of the plate experiences a turbulent flow; the transition is shown in Fig. 21.17, occurring where the local Reynolds number, computed with the distance from the leading edge, reaches a value of 500,000.

In the case of streamlined bodies, it is expedient to maintain a laminar boundary layer as long as possible to reduce friction drag. However, in the case of blunt bodies, it often happens that a laminar boundary layer results in higher drag than a turbulent one. This is due to the fact that in a laminar layer the fluid which is in immediate contact with the surface receives less energy from adjacent layers and tends to slow down more quickly. Particularly in cases where the flow outside the boundary layer slows down and the pressure subsequently increases, a thickening of the boundary layer which eventually results in the detachment of the flow and the formation of a wake takes place. This eventually occurs in the case of the turbulent layer as well, but the energy exchanges due to fluid mixing within the boundary layer help to maintain the flow attached to the surface for a longer distance.

The drag coefficient of a sphere is plotted as a function of the Reynolds number in Fig. 21.18, together with a sketch of the streamlines for the cases of laminar and turbulent flow.

The flow around motor vehicles is always turbulent, owing to the presence of vortices in the air near the ground due to other vehicles and, above all, if there is wind, to the ground and fixed obstacles. Vehicles actually move in what can be defined as the boundary layer of the Earth's surface. Even if it were

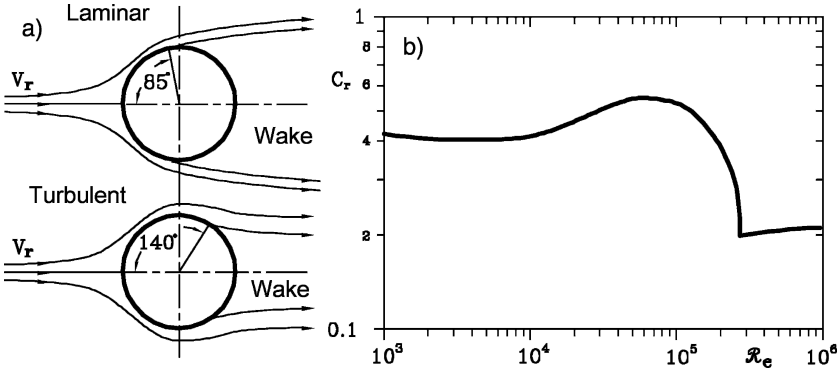

FIGURE 21.18. (a) Qualitative sketch of the streamlines around a sphere. (b) Drag coefficient of a sphere as a function of the Reynolds number.

expedient to keep the boundary layer laminar, it would be very difficult to do so. The percentage of the drag due to friction is usually low, on the order of 10% of the total aerodynamic drag.

21.3.2 Induced drag

Induced drag is that portion of aerodynamic drag that is linked with the generation of lift. In aeronautics, it plays the same role that rolling resistance plays in motor vehicle dynamics: It is responsible for the energy that is dissipated to support the vehicle during motion.

In the case of road vehicles, aerodynamic lift is not needed, and is actually a nuisance. The induced drag should be reduced to a minimum by reducing lift. An exception is the negative lift produced by aerodynamic devices aimed at increasing the normal force holding the vehicle to the ground: In this case, induced aerodynamic drag adds to increased rolling resistance.

To understand the origin of induced drag, reference can be made to the theory of high aspect ratio (the ratio between the span and the chord) wings attributed to Prandtl. This theory can be applied in many cases to the wings which produce negative lift in racing cars. The lift of a wing is directly linked with a difference of fluid velocity between the upper and the lower surface of the wing, which causes a difference of pressure and ultimately a lift force. The difference of velocity can be thought as a vortex superimposed on the uniform airflow (Figure 21.19a).

If the wing had an infinite span, all sections would experience a two-dimensional flow: No induced drag is produced. In the case of an actual finite-span wing, the vortex cannot vanish at the tips of the wing and its core is simply deflected backwards, creating a wake of vortices. To understand intuitively why this vorticity is generated, it must be considered that air under the wing, whose pressure has increased, tend to move toward the tip, where it goes around the end of the wing toward the upper surface, where pressure is lower. The vortex then winds around the tip edge of the wing, a motion that remains even after the wing has passed (or the stream flows beyond the wing, in the wing tunnel model, where the wing is stationary and the air flows around it), producing a trailing vortex.

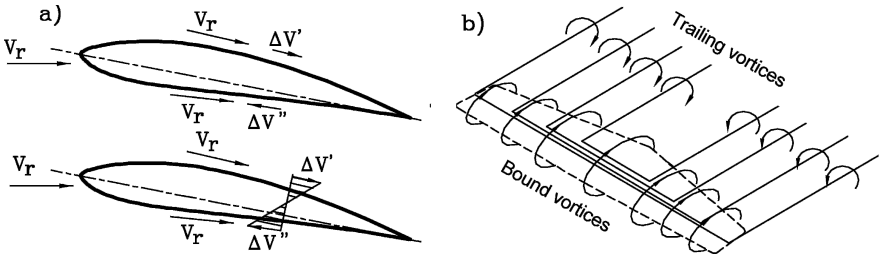

FIGURE 21.19. Vorticity in a lifting wing. (a) Bound vortex; (b) trailing vortices.

A bound vortex plus the two trailing vortices at its end constitute a horseshoe vortex, like those shown in Fig. 21.19b. Since the vorticity is not constant along the wing, a set of such vortices is produced and the trailing vortices depart at different points along the wing. Actually, rather than of a *set* of vortices, we should speak of a *distribution* of vortices.

The energy dissipation needed for the creation of the trailing vortices explains the presence of the induced drag. Any device which reduces trailing vortices, such as tip plates or modified wing tips, is effective in reducing induced drag. Trailing vortices are sometimes easily visible at the tips of the wings of racing cars.

From the theory of high aspect ratio wings it can be deduced that induced drag is proportional to the square of the lift or, which is equivalent, that the induced drag coefficient is proportional to the square of the lift coefficient. However, in the case of low aspect ratio wings and, above all, blunt bodies, this proportionality no longer holds. The presence of the ground can also modify the pattern of vortices. It has been suggested in the case of road vehicles that it is not possible to define an induced drag and that the term vortex drag is preferable[6]. Whatever the case, the vortices which are created behind a vehicle (Fig. 21.9) are linked with the generation of lift, and a reduction of lift always causes a reduction of the overall aerodynamic drag.

21.3.3 Shape drag

Shape drag is what remains of the drag if the contributions due to friction and induced drag are removed and, in the case of road vehicles, it is mainly due to the wake. The pressure in the wake is low and fairly constant and hence shape drag can be approximately evaluated as the product of the wake pressure by the projection on yz plane of the area exposed to it: The shape of the part of the vehicle in the wake has little importance. This statement must not be misunderstood: The shape of the tail of the vehicle is important to assess where the wake starts, but once this issue is solved, only the extension of the wake matters.

Remark 21.5 *Any geometrical irregularity can precipitate the detachment of the flow and the wake formation, particularly if it is located in a zone in which the flow slows down.*

21.3.4 Aerodynamic drag reduction: passenger vehicles

Since the beginning of motor vehicle technology, several attempts aimed at reducing aerodynamic drag have been made. Shapes developed for aircraft and for

[6]R.T. Jones, Discussion on T. Morel, *The effect of base slant on the flow pattern and drag of three-dimensional bodies with blunt ends*, in Aerodynamic drag mechanism of bluff bodies and vehicles, Plenum Press, New York, 1978.

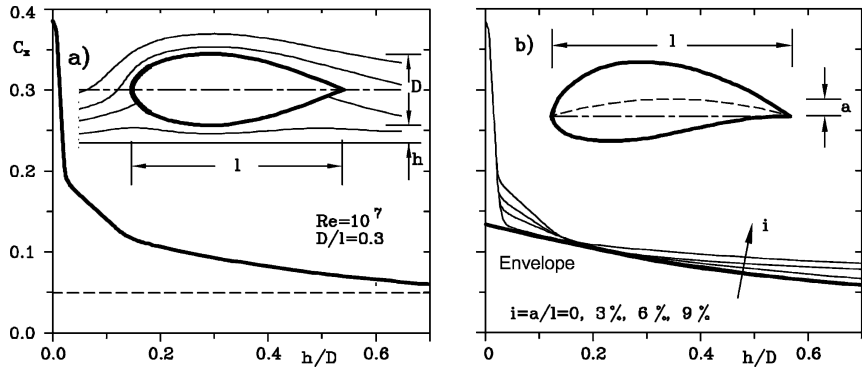

FIGURE 21.20. (a) Streamlines around a straight slender body and values of C_x versus the distance from the ground. (b) Values of C_x versus the distance from the ground for cambered slender bodies with different values of camber.

airships have been adopted, often in a naive way, as the attempt to streamline the body was often offset by mechanical parts completely exposed to the wind.

The shape which proved to produce the lowest ratio between aerodynamic drag and volume was the straight, circular, slender body with a diameter to length ratio equal to about 0.3. For a Reynolds number of about 10^7, its drag coefficient is of 0.05. However, it is difficult to produce a suitable car body from this specification and it is, moreover, optimal only if the vehicle's motion takes place far from the ground. The presence of the latter causes the flow to change substantially (Fig. 21.20a) and the value of C_x to be far higher, up to values of about 0.15 at distances from the ground typical of motor vehicles.

If the vehicle's distance from the ground were zero, the best shape would be half of a slender body, a consideration which seems to have inspired several designs of the past. However, the distance of the vehicle from the ground cannot be zero, and this solution leads to quite high values of the drag.

If the axis of the slender body is curved, a lower resistance to motion near the ground results (Fig. 21.20b), with an optimum value of the camber ratio a/l existing for each value of the distance from the ground. The optimum value of the camber ratio for a nondimensional ground clearance $h/D = 0.1$ is about 10%. However, the difficulties in adapting a slender body to a vehicle and housing the mechanical components and the wheels in it remain.

The results obtained by Lay in 1933 through a series of wind tunnel tests performed on modular models are still interesting. His basic shapes were a flat plate perpendicular to the current (he found a value of C_x larger than 1.2), a slender body (whose C_x was measured at 0.08), a rectangular box ($C_x = 0.86$), and a vehicle from his era ($C_x = 0.6$).

He then discovered that a slight rounding of the corners of the box resulted in a decrease of C_x to 0.46. By fitting different front and rear parts to the vehicle model, he saw not only that by shaping both parts suitably could aerodynamic drag be reduced, but also that the shaping of the rear part is more important

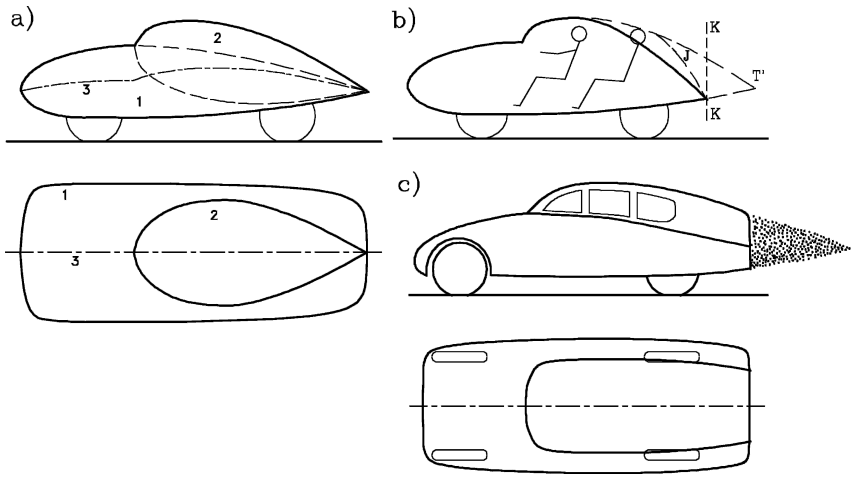

FIGURE 21.21. Streamlined car bodies following J and K shapes. (a) J-shape; (b) problems linked to the length of J-shapes and cutting of the tail; (c) K-shape: One of the drawings from the original patent by Koënig.

than that of the front part. Also, using the shapes tested by Lay, it is necessary to accept a very long vehicle to obtain low drag.

Ten years earlier, in 1923, Jaray obtained a patent in Germany for a car body made by a rectangular cambered stub wing with a slender body superimposed on it (Fig. 21.21a). This approach, named the J-shape, allowed the wheels and other mechanical components to be housed easily, but the problems related to the length of the vehicle, if a sufficient height for the passengers in the rear seats was required, were not solved. The centre line of the body was also quite curved, resulting in non-negligible lift and induced drag. However, the J-shape can be easily identified in many vehicles beginning in the 1950s, like the Lancia Stratos, Citroen DS and many coupé built by Porsche.

In 1937, a new approach was patented almost simultaneously by Kamm and by Koënig and Fachsenfeld Reinhard. From the observation that to obtain optimum height in the back of the J-shape without a very long vehicle, a shape which is prone to produce a large wake is obtained, and that the shape of the part of the vehicle in the wake has little significance, they suggested that the long streamlined tail of the J-shape could be truncated, following line KK of Fig. 21.21b. The result is shown in Fig. 21.21c, from the original patent[7].

Truncation does not affect shape drag, if the part cut off was already in the wake, and likely reduces lift and induced drag. This statement is a rough approximation, since any change in a part of the vehicle changes the entire aerodynamic field, but the use of the K-shape allowed designers to reduce the drag of many passenger vehicles. Many cars of the 1970s had essentially a K-shape, like

[7]Brevetto industriale n. 352583 - Carrozzeria per automobili.

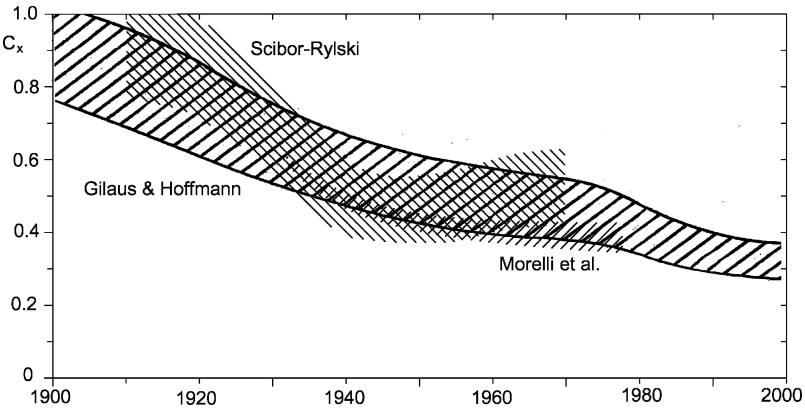

FIGURE 21.22. Experimental values of C_x for passenger vehicles versus the year of construction.

the Citroen GS and CX, Lancia Beta and Gamma, Alfa Romeo Alfasud, Rover 3 liters and many others.

The aerodynamic evolution of passenger vehicles, in terms of the C_x coefficient, is summarized in Fig. 21.22: The three hatched zones refer to plots obtained by different Authors: Gilhaus and Hoffmann[8] refer to cars of different types, Morelli *et al.*[9] report on the drag of cars with a sound aerodynamic shape, many of which were built following the J- or K-shape, while the data reported by Scibor Ryilski[10] are related to a larger sample containing cars of all types. There is no contradiction between them: While the best vehicles showed a constant progress towards low drag, the availability of more powerful engines and the low cost of energy caused a decrease in the movement towards better aerodynamics in the fifties, with an average increase in the drag of cars.

Remark 21.6 *Actually, what really matters is not the value of coefficient C_x, but the value of product SC_x: to reduce drag it is possible to search for a low value of the x-force coefficient or for a shape with low cross sectional area.*

Any device aimed at reducing the value of C_x that causes an increase of the frontal area, like a plate at the rear edge of the roof, is effective only if the decrease of the former is larger than the increase of the latter.

Some values of both coefficient C_x and of the product SC_x, allowing a more direct comparison, for more modern cars are reported in Table 21.2[11]. By comparing the values in the table with those reported in Fig. 21.22, the progress which occurred in the 1980s, mainly linked with the increase of the cost of energy

[8] A. Gilhaus and R. Hoffmannm, *Directional stability,* in W.H. Hucho (Ed.), *Aerodynamics of Road Vehicles*, SAE, Warrendale, 1998.

[9] A. Morelli, L. Fioravanti, A. Cogotti, *Sulla forma della carrozzeria di minima resistenza aerodinamica*, ATA, Nov. 1976.

[10] A.J. Scibor Ryilski, *Road Vehicle Aerodynamics*, Pentech Press, London, 1975.

[11] H.P. Leicht, *Kanal voll* , Auto-motor sport, 18/1986.

TABLE 21.2. Values of C_x. S and product SC_x for some European cars.

	$C_X S$ [m^2]	C_X	S [m^2]		$C_X S$ [m^2]	C_X	S [m^2]
Lancia Y10	0.57	0.33	1.76	Opel Corsa SR	0.61	0.35	1.73
Fiat Uno	0.62	0.34	1.83	VW Polo	0.65	0.38	1.70
Renault 5	0.67	0.37	1.80	Austin Metro	0.67	0.39	1.73
Peugeot 205	0.68	0.39	1.74	Fiat Panda	0.70	0.41	1.70
Citroen Visa	0.70	0.40	1.75	Ford Fiesta	0.73	0.41	1.76
Renault 4	0.90	0.49	1.83				
Opel Kadett GSi	0.60	0.32	1.88	Peugeot 309	0.64	0.34	1.86
VW Golf GL	0.65	0.34	1.89	Mercedes 190 E	0.65	0.34	1.89
Renault 21	0.66	0.34	1.94	Ford Sierra XR 4i	0.67	0.34	1.98
VW Golf GTI 16V	0.67	0.35	1.91	Citroen BX	0.68	0.36	1.91
VW Jetta CL	0.68	0.36	1.89	VW Passat GL	0.70	0.37	1.90
Fiat Ritmo	0.70	0.37	1.88				
Opel Omega	0.58	0.28	2.06	Mercedes 200	0.60	0.29	2.07
Audi 100	0.62	0.30	2.05	Renault 25	0.62	0.31	2.03
Ford Scorpio	0.70	0.35	2.02	Fiat Croma	0.70	0.34	2.04
Lancia Thema	0.73	0.36	2.06	Honda Prelude 16V	0.76	0.41	1.84
Alfa 90	0.77	0.40	1.92	Citroen CX	0.78	0.40	1.96
Mitsubishi Galant	0.79	0.40	1.98				
Ferrari Testarossa	0.61	0.33	1.85	Mercedes 190 E2.3	0.64	0.33	1.94
Porsche 944 turbo	0.65	0.35	1.89	VW Scirocco 16V	0.68	0.38	1.78
Porsche 911 Carrera	0.68	0.38	1.77	Mitsubishi Starion T	0.69	0.37	1.84
Alfa Romeo GTV	0.71	0.40	1.77	Jaguar XJ-S	0.73	0.40	1.83
Porsche 928 S	0.77	0.39	1.96	Audi Quattro	0.80	0.43	1.86
BMW M 635 CSi	0.80	0.40	2.00				

which took place a decade earlier, is clear. It must be noted, at any rate, that with a few exceptions, the values of C_x are rarely lower than 0.35, with many cars having a value between 0.35 and 0.45.

The search for a shape of minimum drag for any particular vehicle can be approached by identifying a number of critical details and optimizing them one by one. The principle of effects superimposition cannot be applied in aerodynamics; the drag of a body is not the sum of the drag of all its parts, and any change to one of them causes a change in the drag of all others. However, it is a common practice to obtain the drag of a body as the sum of the drag of its parts plus a further component, referred to as interference drag. This approach has been successfully used first in aeronautics and then in road vehicle technology.

A method, known as detail optimization is now widely used. It is based on subsequent detail modifications to achieve drag reductions which can be quite substantial. The drag coefficient of the base shape is measured and a number of specific details of the car body are chosen. One of them is modified and the wind tunnel test is repeated, with modifications continuing until a minimum of the drag is obtained. The work is then repeated for all the chosen details. This procedure can be thought as the search for the minimum of a function (drag) of many variables (the geometrical characteristics of the details), by modifying the value of each one of the variables one at a time, looking for a local minimum in a two-dimensional space and then proceeding to search for a local minimum in a multi-dimensional space. We are not saying that an absolute minimum can be reached in this way, nor even that a relative minimum can be obtained unless an iterative procedure is used, but it is certain that a decrease in drag is eventually obtained.

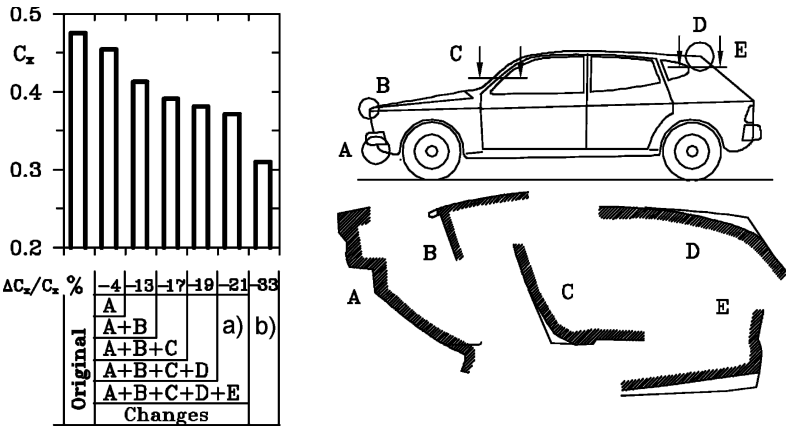

FIGURE 21.23. Detail optimization method. Definition of the five details used to optimize the shape and to reduce the C_x coefficient. (a) Optimized shape, (b) modified shape.

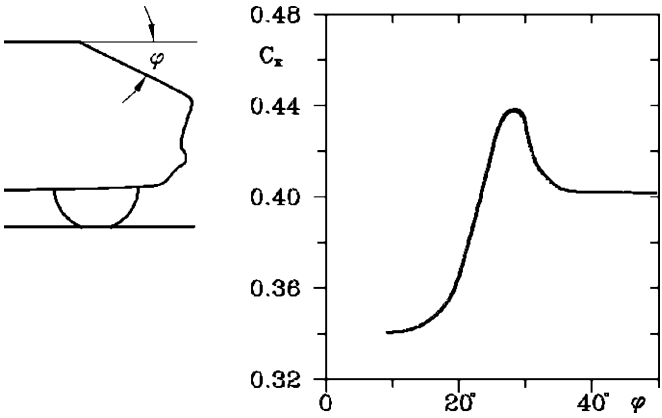

FIGURE 21.24. Coefficient C_x as a function of the angle between the rear window of a given car and the horizontal.

An example is shown in Fig. 21.23, where the base shape and five details are shown. The thin line gives the initial configuration while the thick one describes the optimized shape. By operating in the way above, the drag was reduced by about 21%, while a more substantial reduction of 33% could be achieved only by introducing modifications which changed to a larger extent the overall appearance of the car.

The results obtained by changing the inclination of the rear part of a hatchback car are shown in Fig. 21.24: If the angle between the rear window and the horizontal is larger than 35° the value of C_x is 0.4. With a low value of the angle it is possible to reduce the drag, with a coefficient of about 0.34, but there is a region, at about 28° where large vortices produce a substantial increase in drag,

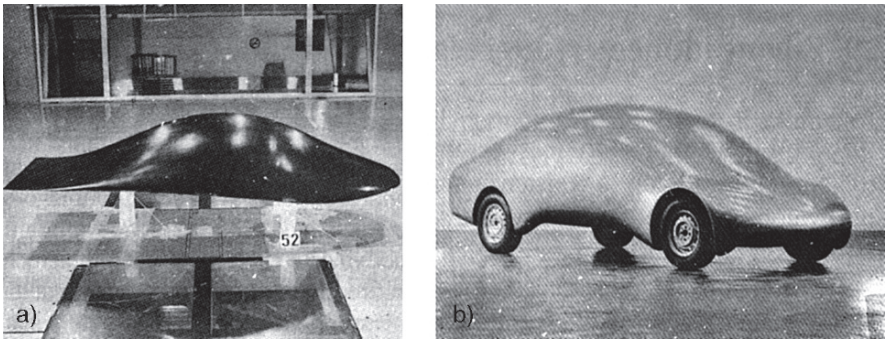

FIGURE 21.25. Ideal and actual shape for a very low-drag research vehicle, shown in the wind tunnel.

up to $C_x = 0.44$. This result confirms the already mentioned results obtained from slanted rectangular blocks.

The advantage of this procedure is in leaving stylists free to design the vehicle without inhibiting their creativity, while obtaining a shape with low drag without drastically changing the aesthetic impact of the car.

Alternatively, it is possible to develop from theoretical considerations ideal shapes aimed at reducing drag to a minimum, modifying these ideal shapes when adapting them to motor vehicle use. An example of this procedure is shown in Fig. 21.25, where both the ideal shape and the car derived from it are represented[12]. The ideal shape has been obtained by specifying that the lift and pitching moment must be zero, the positive pressure gradients must be as low as possible, the cross section of the body must vary slowly in shape and area, and its contour must be rounded as much as possible.

The value of C_x of the ideal body in the vicinity of the ground proved to be as low as 0.049, the same as that of a slender body located at an infinite distance from the ground. The vehicle obtained from it had a value for C_x of only 0.23, while maintaining a satisfactory internal space for the occupants, the luggage and the mechanical components, not unlike a regular saloon car.

As a result of research performed in the eighties in many countries, it is possible to state that values of coefficient C_x as low as 0.25 can be achieved without excessive sacrifice to the internal space and general characteristics of the vehicle. The success of detail optimization procedures allowed designers to overcome fears, expressed several times in the 1970s, that aerodynamic studies would cause all cars to look alike, and that the image of individual manufacturers would be sacrificed to the need for good aerodynamic performance.

It is also clear, however, that the lower the drag coefficient is, the fewer are the advantages of further reductions in fuel consumption, particularly since

[12]CNR, Progetto Finalizzzato Energetica, Atti del primo seminario informativo, Torino, Aprile 1978 and A. Morelli, L. Fioravanti, A. Cogotti, *Sulle forme della carrozzeria di minima resistenza aerodinamica*, ATA, Nov. 1976.

the average use of road vehicles occurs at speeds lower than those at which aerodynamic drag is the most important form of resistance to motion.

As the actual average speed of driving depends mostly on issues unrelated to the design of vehicles themselves (road conditions, laws and their enforcement etc.), at present the search for very low drag is not pushed to extremes, at the expense of other characteristics, mainly aesthetic, in the design of passenger vehicles.

21.3.5 Aerodynamic drag reduction: industrial vehicles

Even in the recent past, industrial vehicles have usually been designed with little concern for their aerodynamic characteristics. The low speed and the high value of the ratio between the mass and the frontal area renders the power needed to overcome aerodynamic drag a small fraction of the total power needed for motion. However, the higher speeds industrial vehicles reach on highways and increased concern about energy saving have led to many studies aimed at reducing the drag in this field as well.

In the case of single-body vehicles, such as buses, vans and trucks without a trailer, the basic shape is essentially a square box. If the edges are blunt, the value of C_x is in the range 0.82–0.86, mostly owing to the fact that the flow is widely separated and the wake is very large (Fig. 21.26).

From this figure it is clear that any change of shape allowing flow separation to be reduced is very beneficial: Simply by rounding the edges slightly, the drag coefficient can be reduced almost by half, to about 0.45.

With an improved frontal profile, values in the range $0.4 \div 0.43$ may be obtained for buses and vans. It is difficult to lower this value further. Fairings on the underside may make it possible to lower it by about 0.05, but many other devices aimed at increasing the pressure in the wake have been tried without success.

Tests on models have shown even greater reductions of drag: by simple rounding of the corners with a 150 mm radius, a value as low as $C_x = 0,36$ has been obtained.

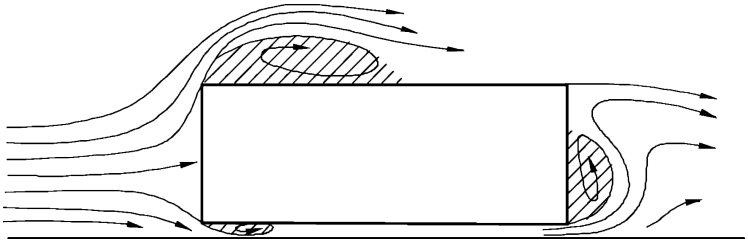

FIGURE 21.26. Streamlines around a square box with blunt edges, at a distance from the ground equal to 0.06 D, where D is the diameter of a circle having the same cross-sectional area of the body.

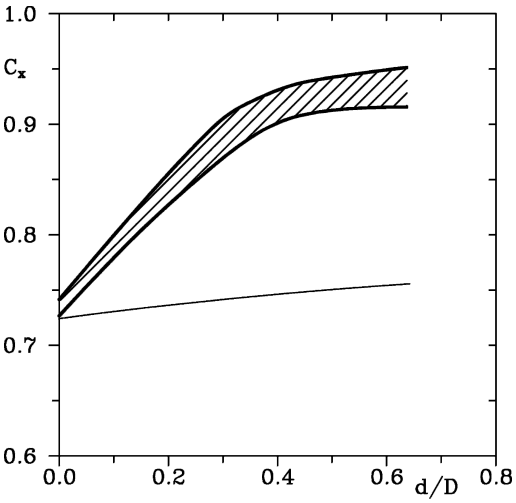

FIGURE 21.27. Values of the coefficient C_x versus ratio d/D for articulated vehicles with different cab shapes. d is the distance between the cabin and the semitrailer and D has the same meaning as in the previous figure.

Two flow stagnation points can be present in articulated vehicles, one on the cab and one on the trailer, with a flow occurring in the space between the two bodies. The drag depends largely on their distance d, as shown in Fig. 21.27, referring to articulated trucks. The dashed zone contains experimental points obtained with differently shaped cabs.

The value of C_x increases from about 0.72 to about 0.93 when the distance grows from $d = 0$ to $d = 0.6$. To reduce drag, the flow between cab and trailer must be blocked to create a single stagnation point; the simplest way is to put a vertical flat plate on the roof of the former (the thin line in Fig. 21.27).

The flow is similar to that characterizing the situation with $d = 0$; there is a single stagnation point on the tractor and a separation bubble between the two bodies. A second separation bubble is formed on the roof of the trailer, owing to the front edge of the latter. Further decrease of drag may be obtained using shaped deflectors on the roof of the cab.

Vertical flat plates can be put on the roof of the cab (e.g. made by the front side of the air conditioner box) or the plates may be true, shaped deflectors. At any rate, their size must be such that the flow reattaches at the front edge of the trailer (Fig. 21.28c). The planform of the cab must also be designed so that there is no separation on the sides of the trailer. By using such deflectors it is possible to reduce C_x below 0.6.

Rounding the edges of the trailer is effective, in that it makes the partitioning of the deflector on the tractor less critical, avoiding the detaching of the flow if the deflector is too low. At any rate it is more important designing correctly the tractor and rounding the edges of the trailer than streamlining the two parts independently.

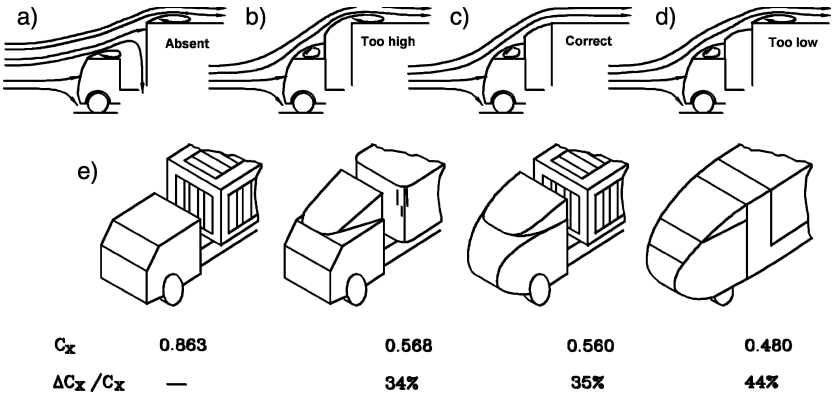

FIGURE 21.28. (a-d) Flow on the front part of an articulated truck with and without a flat plate (air deflector) on the cab. (e) Reduction of the drag of articulated vehicles; values obtained on half-size models.

Some results obtained on half scale models are shown in Fig. 21.28e; they show that with just few modifications, including a deflector, a large reduction is readily obtained, while further improvements are difficult to achieve and require a global streamlining of the vehicle. A value of C_x of about 0.5 can thus be obtained; lower values, down to 0.24 as obtained on a 1/10 scale model, could be achieved by using a complete fairing of the underside.

The above mentioned values of C_x all referred to vehicles driven with no aerodynamic sideslip angle. If β_a is not zero, the aerodynamic field and its associated aerodynamic forces and moments are quite different. This is true for all vehicles, but holds in particular for industrial vehicles, since the lower speed they usually travel increases the significance of side winds, even those of moderate strength. As an example, a wind perpendicular to the road blowing at $V_a = 10$ km/h causes an aerodynamic sideslip angle $\beta_a = 8°$ in the case of a vehicle travelling at $V = 70$ km/h.

A qualitative plot of C_x as a function of β_a for a generic industrial vehicle is shown in Fig. 21.29a. It must be stressed, however, that if sidewind is present, the sideslip angle β is not zero. The aerodynamic force F_x is then not exactly aligned with the velocity V, and the power needed for overcoming aerodynamic drag is $F_x V \cos(\beta)$ plus the component of the side force F_y in the direction of velocity V. Moreover, the rolling resistance of the tires increases due to the sideslip angle of the wheels.

The aerodynamic drag of articulated vehicles increases strongly with the aerodynamic sideslip angle β_a for angles between 0 and 20°. This increase is particularly noticeable for articulated trucks with aerodynamic devices aimed at preventing airflow between tractor and trailer. When lateral wind is present a flow of air in transverse direction between the cab and the trailer can be created and the advantages obtained by using deflectors end up disappearing for values of β_a of about 20°. Curved deflectors work better from this viewpoint than flat

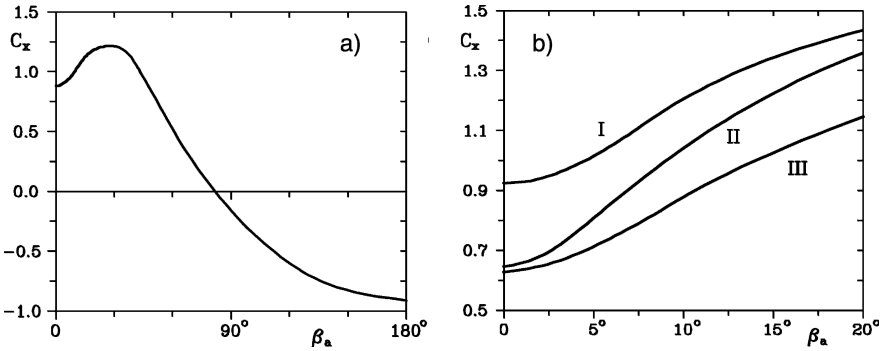

FIGURE 21.29. (a) Coefficient C_x versus sideslip angle β_a for an articulated truck. (b) Effects of drag reducing devices on the curve $C_x(\beta_a)$: I no deflector; II flat plate deflector; III deflector and round front edges of the trailer.

plates, which usually cause an increase of drag at even low values of β_a. Curves $C_x(\beta_a)$ for articulated trucks with different aerodynamic devices are shown in Fig. 21.29b. As shown, the use of deflectors must be accompanied by the rounding of the edges of the trailer.

21.4 LIFT AND PITCHING MOMENT

Apart from the drag increase due to induced drag, aerodynamic lift must be avoided since it reduces the load on the tires and consequently the forces the vehicle can exert on the ground; moreover, this reduction is strongly dependent on the speed. In the case of vehicles with high power/weight ratio, it is possible to use negative aerodynamic lift to enhance power transfer through the road-wheel contact. The same holds for increasing the cornering forces.

In addition, aerodynamic pitching moment M_y must be as small as possible, since it causes strong variations in the forces exerted by the wheels on the road, that depend on speed. With reference to Fig. 21.30, the pitching moment is positive when it acts to increase the load on the front wheels. As the aerodynamic drag is applied to the centre of mass, at a distance h_G from the ground, the longitudinal load transfer on a vehicle with two axles is

$$\begin{cases} \Delta Z_1 = \dfrac{1}{2}\rho V^2 S\left(C_{M_y} - \dfrac{h_G}{l}|C_x| - \dfrac{b}{l}C_z\right) \\ \Delta Z_2 = \dfrac{1}{2}\rho V^2 S\left(-C_{M_y} + \dfrac{h_G}{l}|C_x| - \dfrac{a}{l}C_z\right). \end{cases} \tag{21.18}$$

Instead of speaking of lift and pitching moment, the lift is often subdivided on the two axles and a front axle F_{z1} and rear axle F_{z2} lift are defined. Similarly, the lift coefficient C_z is split into two coefficients C_{z1} and C_{z2} with reference to the axles. The evolution in time of C_z in passenger cars, split into its components

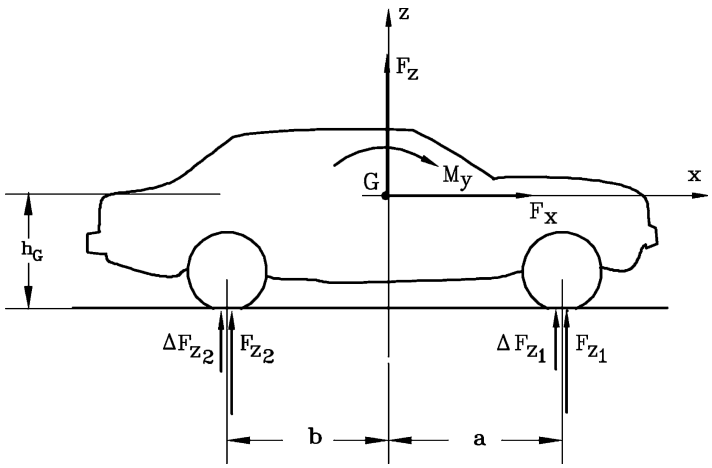

FIGURE 21.30. Longitudinal load transfer due to aerodynamic pitching moment and lift. Forces F_z and ΔF_{z_i} are the forces the vehicle receives from the ground; a positive ΔF_z indicates an increase of load.

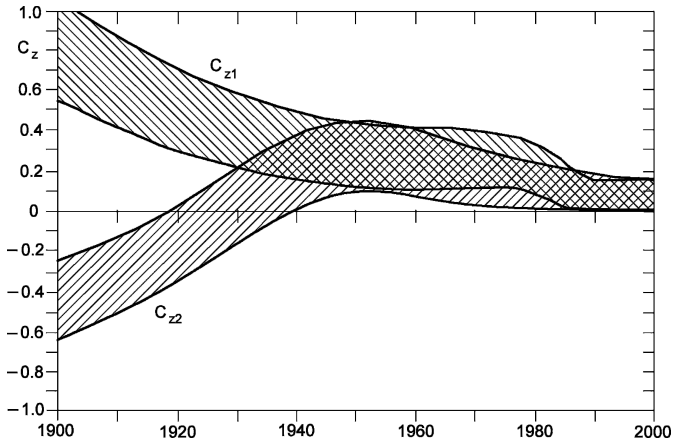

FIGURE 21.31. Evolution in time of coefficient C_z, split in its components on the front and rear axles.

on the axles, is summarized in Fig. 21.31[13]. Lift has remained small and positive (directed upwards), with a good reduction in recent years, while the average pitching moment was negative (tending to lower the load on the front axle) up to the 1940s, to decrease in later years.

Aerodynamic lift and pitching moment depend on the position of the vehicle on the ground, primarily on the aerodynamic angle of attack α, that in the

[13]A. Gilhaus and R. Hoffmannm, *Directional stability,* in W.H. Hucho (Ed.), *Aerodynamics of Road Vehicles*, SAE, Warrendale, 1998.

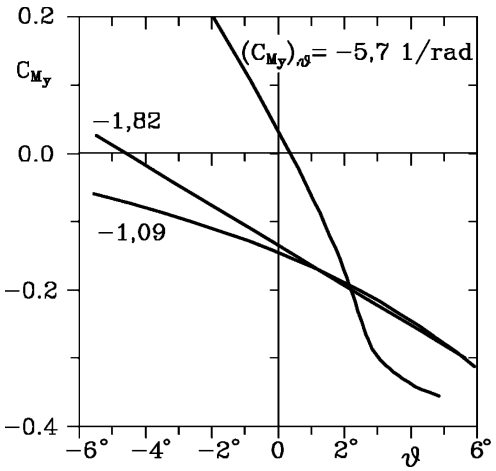

FIGURE 21.32. Pitching moment coefficient C_{M_y} as a function of angle θ for three different vehicles.

following pages is assumed to coincide with the pitch angle θ. Lift can be considered as varying linearly for small changes of α (or θ), and both C_z and $\partial C_z/\partial\theta$ must be measured in the wind tunnel. The same holds for the pitching moment. A plot of the moment coefficient C_{M_y} versus angle θ for 3 different vehicles is reported in Fig. 21.32; the values of the derivative $\partial C_{M_y}/\partial\theta$ (indicated as $(C_{M_y})_{,\theta}$) for small movements about the reference position are also reported. Note that the moment and its derivative are mostly negative; this is a general rule.

To reduce the lift, and in some cases to make it negative, many current passenger vehicles are provided with spoilers on the rear part of the body or on the front bumper. Apart from the obvious consideration that their position and size must be accurately studied in the wind tunnel since they are useless if located in the wake or in other zones in which the flow is detached, they must be placed in such a way as to avoid giving way to pitching moments.

A spoiler usually creates some shape drag, as it increases the size of the wake, but it can be effective in reducing the total aerodynamic force F_x owing to reduction of the induced drag (Fig. 21.33).

Since spoilers cause an increase of pressure on the tail of the vehicle, they usually create a positive pitching moment. This moment must be compensated by another surface positioned near the stagnation point, usually referred to as a bumper spoiler, air dam or apron. Its presence is also usually beneficial on drag.

Strong negative lift forces are obtained in racing cars both by the use of wings and by a suitable aerodynamic design of the whole body. Usually there is a rear wing, which may have a multiplane configuration, and a front wing, integrated with the nose of the vehicle. The airflow in the zone where these wings are located is strongly influenced by the rotation of the wheels and their

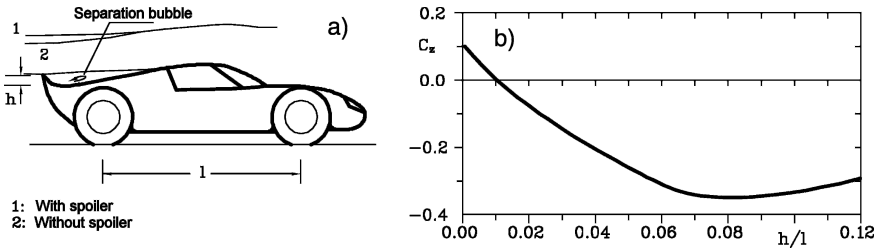

FIGURE 21.33. Lift reducing devices. Effect of a deck-lid spoiler on the streamlines (a) and on the values of the lift coefficient (b).

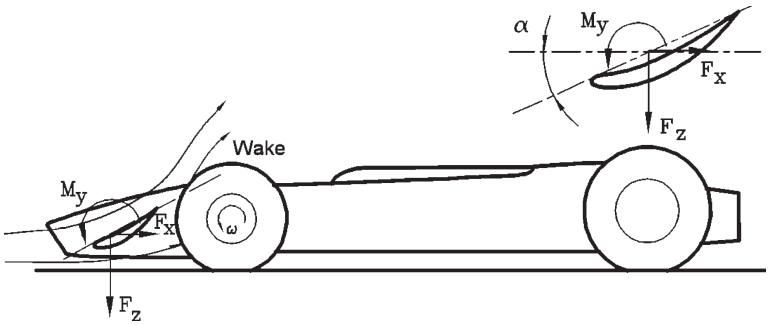

FIGURE 21.34. Forces and moments acting on the wings of a racing car. Interference between wings and rotating wheels.

actual angle of attack, i.e. the angle between the surface and the direction of the impinging current may be quite different from the geometrical angle of attack (Fig. 21.34). Each of the wings produces a negative lift, a drag, usually quite strong, and a pitching moment. These must combine in such a way that the total pitching moment acting on the car is as small as possible.

The entire body of a racing car can be designed to produce negative lift; in fact if the pressure under the vehicle is lower than atmospheric pressure, strong downwards forces may be exerted on the underside. Many racers were based on this concept, with the whole vehicle body designed as a sort of upside-down wing. Suitable side walls, almost reaching the ground, channelled air below the vehicle, producing an area of low pressure and then negative lift. Since aerodynamic devices have a strong impact on safety, racing regulations deal with them in detail. Since 1983, exploiting ground effect it is no longer allowed and the bottom of the car must be flat. Since regulations change often, it is impossible to give general rules on the devices used on racers to produce negative lift.

21.5 SIDE FORCE AND ROLL AND YAW MOMENTS

If the vehicle has a symmetry plane and is in a symmetrical position with respect to the airflow, i.e. if the roll and the aerodynamic sideslip angles are equal to zero, the side force F_y, the rolling moment M_x and the yawing moment M_z vanish. In general, what matters is their rate of change with angle β_a and, sometimes, roll angle ϕ. In the case of racing cars with uncovered wheels, these forces can also be produced by offset steering wheels and it is important to study their variation with the steering angle δ.

For small variations of the mentioned parameters about zero, coefficients C_y, C_{M_x} and C_{M_z} can be approximated by linear functions and their derivatives $(C_y)_{,\beta_a}$, $(C_{M_x})_{,\beta_a}$, etc. can be considered constant.

Some typical curves $C_y(\beta_a)$ are reported in Fig. 21.35a. The slope of the curve in the origin is –2.2 rad^{-1} for a typical American saloon car and –2.85 rad^{-1} for a sport car. For a first approximation evaluation of the slope $(C_y)_{,\beta_a}$ (in rad^{-1}), the following formula has been suggested

$$(C_y)_{,\beta_a} = \frac{\text{lateral area}}{\text{front area}}\left(0.005 + 0.0019 n_f\right), \tag{21.19}$$

where n_f is a numerical factor which must be obtained from experimental results on vehicles similar to the one under study. As already stated, $(C_y)_{,\delta_a}$ is usually small, except for racing cars. On some Formula 1 racers a value of 1.37 rad^{-1} has been recorded[14].

Even more important than the side force, the aerodynamic yawing moment M_z plays a key role in the dynamics of high speed driving. The evolution of coefficient C_{Mz} in passenger cars is summarized in Fig. 21.36[15].

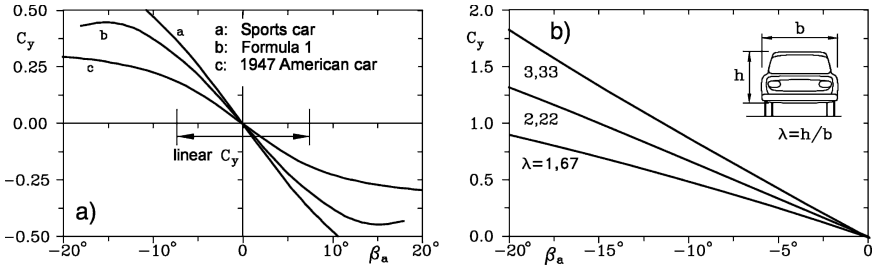

FIGURE 21.35. Coefficient C_y versus angle β_a. (a) Typical values for vehicles of different types; (b) dependence on the ratio width/height of the vehicle.

[14] A.J. Scibor Rylski, *Road Vehicle Aerodynamics*, Pentech Press, London, 1975.

[15] A. Gilhaus and R. Hoffmannm, *Directional stability,* in W.H. Hucho (Ed.), *Aerodynamics of Road Vehicles*, SAE, Warrendale, 1998.

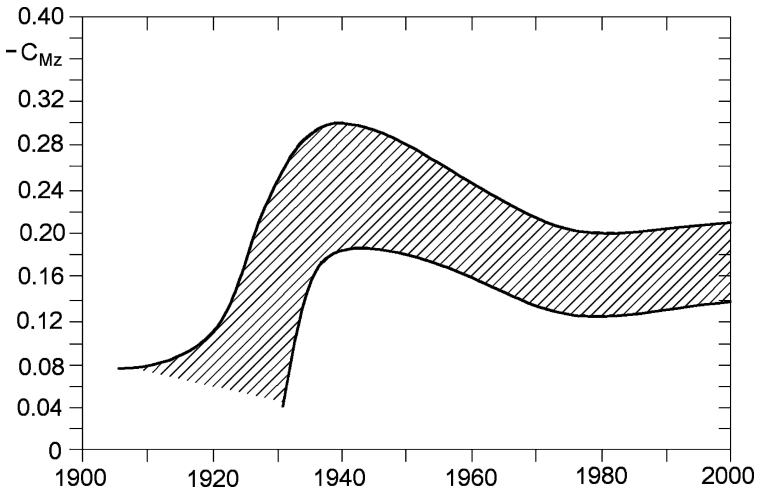

FIGURE 21.36. Evolution in time of coefficient C_{Mz}. Values for an aerodynamic sideslip angle $\beta_a = 20°$.

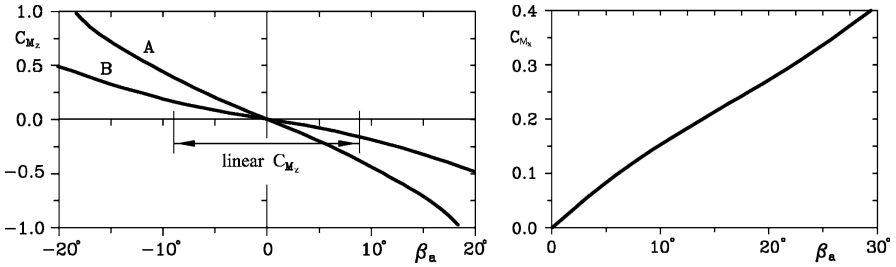

FIGURE 21.37. (a) Typical laws $C_{M_z}(\beta_a)$ for a well streamlined car (A) and a car with a less careful aerodynamic design (B). (b): Rolling moment coefficient C_{M_x} versus β_a for a typical saloon car.

Remark 21.7 *A reduction of aerodynamic drag, in particular if low drag is obtained even at high values of the sideslip angle, is usually detrimental for the lateral force and above all the yawing moment.*

Some typical laws $C_{M_z}(\beta_a)$ are reported in Fig. 21.37a: Usually the moment is negative for a positive sideslip angle, which amounts to saying that the side force is applied in a forward position with respect to the centre of mass. This arrangement, which occurs very often, is destabilizing at high speed; the value of C_{M_z} may be large enough to cause force F_y to be applied in front of the vehicle.

A nonlinear expression for coefficient C_{M_z} is

$$C_{M_z} = -\left[K - \sin^2(\beta_a)\right] \tan(\beta_a) \,, \tag{21.20}$$

TABLE 21.3. Changes of the aerodynamic coefficients due to objects carried on the roof of a saloon car. Coefficients referred to the front surface of the base car.

	C_x	C_{z_1}	C_{z_2}	C_y	C_{M_z}	C_{M_y}	C_{M_x}
	$\beta = 0$			$\beta = 20^\circ$			
Car	0.34	0.09	0.19	0.66	0.17	0.13	0.12
Roof rack	0.38	0.10	0.12	0.74	0.16	0.16	0.13
Ski	0.46	0.08	0.13	0.76	0.15	0.15	0.15
Surf board	0.47	0.10	0.13	0.77	0.16	0.16	0.17
Box	0.46	0.10	0.15	0.92	0.15	0.23	0.23
Boat	0.55	0.24	−0.03	1.12	0.17	0.37	0.30
Bycycle	0.55	0.19	0.03	1.00	0.12	0.32	0.38

where constant K, whose obvious meaning is the value of $(C_{M_z})_{,\beta_a}$ in the linear part of the plot, must be obtained from vehicles similar to the one under study. MIRA[16] suggests for $(C_{M_z})_{,\beta_a}$ the expression

$$(C_{M_z})_{,\beta_a} = -\frac{1}{100}\left[\frac{\text{lateral area}}{\text{front area}}(0.208 + 0.0655 n_f - 0.00508 n_f^2)\right] , \qquad (21.21)$$

where n_f must again be obtained from experimental data.

For $(C_{M_z})_{,\delta}$ the same considerations seen for $(C_y)_{,\delta}$ hold; an order of magnitude for Formula 1 racers is a value of 0.46 rad^{-1}.

A plot of the aerodynamic rolling moment coefficient versus the sideslip angle for a typical saloon car is shown in Fig. 21.37b. From the graph a value of the derivative $(C_{M_x})_{,\beta_a}$ for the linear part of 1.05 rad^{-1} can be obtained.

The presence of external loads on the roof of a car deeply changes aerodynamic performance. Obviously it increases drag, but it also decreases lift, above all at the rear axle; in addition, it increases pitching moments and increases sensitivity to side wind. The aerodynamic coefficients of a saloon car with different roof loads are reported as an example in Table 21.3.

21.6 EXPERIMENTAL STUDY OF AERODYNAMIC FORCES

The traditional tool for the study of aerodynamic forces and moments is the wind tunnel. Modern wind tunnels used for road vehicle aerodynamics are specialized devices, quite different from those used in aeronautics. Wind tunnel tests of cars are almost always performed on full-size vehicles, since it is very difficult to simulate with the required precision internal flows on reduced scale models.

Wind tunnels for vehicular use are divided into aerodynamic and climatic tunnels.

[16] R.G.S. White, *A rating method for assessing vehicle aerodynamics side force and yawing moment coefficients*, MIRA Rep. n. 1, 1970.

The first of these are designed to simulate the aerodynamic field for the measurement of aerodynamic forces and moments, of pressure distribution, etc. and their main requirement is an accurate simulation of the aerodynamic field surrounding the moving vehicle.

Climatic tunnels are used to simulate motion in various climatic conditions, by controlling the temperature of the air and often its humidity. Provisions for producing rain, snow, various sun conditions, etc. are often included. Usually it is possible to run the engine and brake the driving wheels to study, in a realistic way, the temperature conditions in the engine compartment and the working of the cooling and air conditioning systems. The simulation of the aerodynamic field may be less accurate.

Sometimes the two functions are be combined in a single aerodynamic and climatic tunnel, but the convenience of building a single plant for the two tasks instead of two different tunnels must be assessed in each case, keeping in mind above all the compatibility of the balance that measures aerodynamic forces and moments with the rollers that brake the driving wheels.

Climatic tunnels allow the vehicle to be tested in extreme conditions without the need for moving instrumentation and personnel to distant, uncomfortable places, or waiting for extreme climatic conditions to occur in a given place.

The main tests that can be performed in aerodynamic tunnels are:

- Measurement of aerodynamic forces and moments. The three components of both force and moment are measured using a six-component balance.
- Visualization of the airflow around and inside the vehicle and measurement of the pressure at given points of the surface or in other points of the aerodynamic field. Other measurements aimed at understanding the aerodynamic field.
- Measurement of aerodynamic noise, possibly when other sources of noise (engine, transmission, etc.) are present.

Climatic tunnels allow tests to be performed on the behavior of the body (waterproofing, accumulation of dirt, ice formation, weathering, etc.) and of mechanical parts (cooling of engine, starting, air conditioning, operation of the electric devices, etc.) in various climates. Climatic tunnels must be large enough to allow full scale vehicles to be tested, and they must have rollers to brake the wheels and simulate inertias to properly simulate road loads on the driving wheels. The latter device makes it difficult to build tunnels that include a balance for the measurement of forces and moments.

Aerodynamic tunnels for motor vehicles also have a similar size, for as we have seen, the use of models in motor vehicle aerodynamics leads to much less accurate results.

Wind tunnels may be of the open or closed circuit type. While in the former the fan must supply all the kinetic energy of the stream, in closed circuit tunnels some of the kinetic energy of the air that flows around the vehicle is recovered, and the motor needs to supply to the flow only an energy equal to the losses.

The efficiency, defined as the ratio between the power of the airstream and the motor power

$$\eta = \frac{\frac{1}{2}\rho V^3 A}{P} \ , \tag{21.22}$$

of closed circuit tunnels is higher than that of open circuit ones, and is often higher than one.

Open circuit tunnels are simpler, smaller and cheaper but are energetically less efficient. A cost trade-off for the two types of plant must be performed in each case.

While in the aeronautical field most wind tunnels are of the closed circuit type, modern plants for vehicular use are mostly open, perhaps with air recirculation within the building to avoid the need of filtering large quantities of air and to reduce noise pollution to the environment. Recirculation can also increase energy efficiency.

To perform aerodynamic tests on vehicles, high airspeeds are not needed, since a speed of about 10 m/s is high enough to reach values of the Reynolds number of about 2 or 3 million. Tests are generally performed at a speed of 20 or 30 m/s, creating strong enough aerodynamic forces to allow easy and precise measurements.

Climatic tunnels must reach higher speeds, close to the maximum speed of the vehicle. Since the test chamber of wind tunnels for road vehicles has a sectional area of about $10 \div 30$ m^2, the motor must have a power of several hundred or thousand kW. In climatic closed circuit (or open circuit with recirculation of air) tunnels, the power of the refrigerators must be higher than that of the motors, at least if low temperature tests at top speed must be performed.

The type, shape and size of the test chamber is of primary importance in aerodynamic wind tunnels. The aerodynamic field around the test object must simulate as accurately as possible that occurring in free air, and this is easier if the test chamber is large, or rather if the value of the ratio between the area of the air jet and the area of the cross section of the test object is high.

On the other hand, it is clear that the smaller the size of the jet, the lower the power required, as well as the size and cost of the whole plant. The shape of the cross section of the test chamber must be accurately chosen to obtain the required precision with as small a jet as possible. This consideration is, however, mitigated by the fact that a test chamber with rounded walls is much more costly than a rectangular one, so that a rectangular jet is often used, even if by doing so a larger wind tunnel, with greater power requirements, is needed.

The designer of a wind tunnel must choose between an open or closed test chamber. Closed test chambers, like the ones used in most aeronautical wind tunnels, have lower losses but usually require larger jet areas to obtain the same precision in the simulation of the aerodynamic field. Taking both factors into account, closed test chambers require greater power, at least in automotive wind tunnels. An alternative is the use of closed test chambers with porous walls, that is walls allowing a certain quantity of air to be extracted from the flow, with

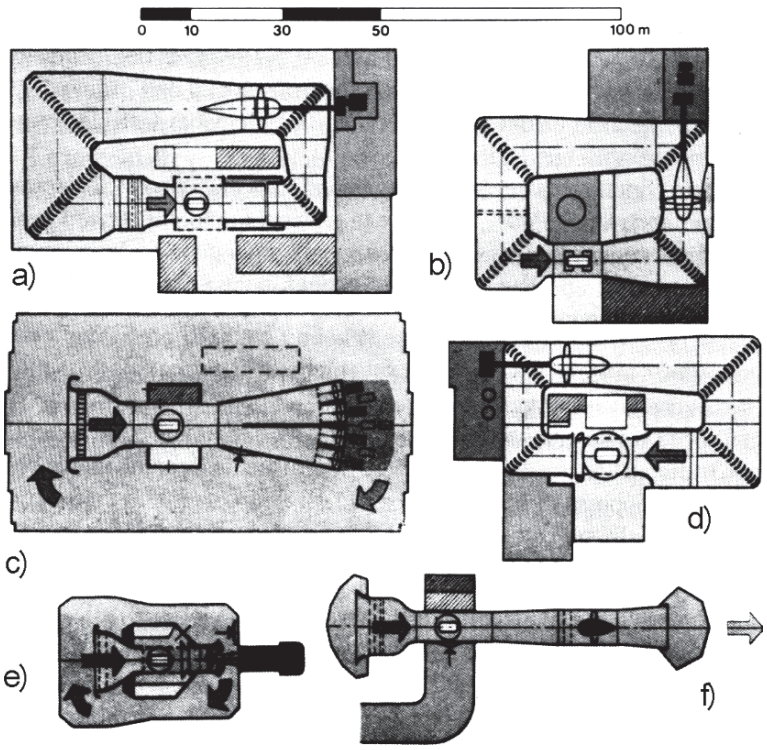

FIGURE 21.38. Plans of six wind tunnels for full-scale testing of road vehicles. (a)Volkwagen, Wolfsburg, Germany; (b) Ford, Detroit, USA; (c) F.K.F.S., Stuttgard, Germany; (d) Pininfarina, Torino, Italy; (e) M.I.R.A., Lindley Nuneaton, G.B., (f) Nissan, Oppama Yokosuka, Japan.

consequent reduction in the thickness of the boundary layer. Another possibility is the use of adaptive test chambers, in which a number of actuators allow the shape of the test chamber to be changed so that the streamlines at a certain distance from the vehicle are similar to those occurring in a free flow.

Sketches of six of the most important vehicular wind tunnels are plotted in Fig. 21.38. Three of them have a closed circuit and three are open, two with air recirculation. The cross section of the Pininfarina wind tunnel is shown in Fig. 21.39, as an example of a modern climatic aerodynamic tunnel with open circuit and air recirculation and open test chamber.

Peculiar difficulties encountered in wind tunnel testing of vehicles are linked with the presence of the ground. To simulate the motion of the ground with respect to the vehicle, a sort of carpet moving at the speed of the air should be used, with the wheels rolling on it. This approach has many drawbacks, particularly in terms of wheel rotation. If the vehicle is kept at a small distance from the ground and the wheels are moved by motors inside the vehicle or model, a flow of air between the wheels and the ground would result and the resulting negative

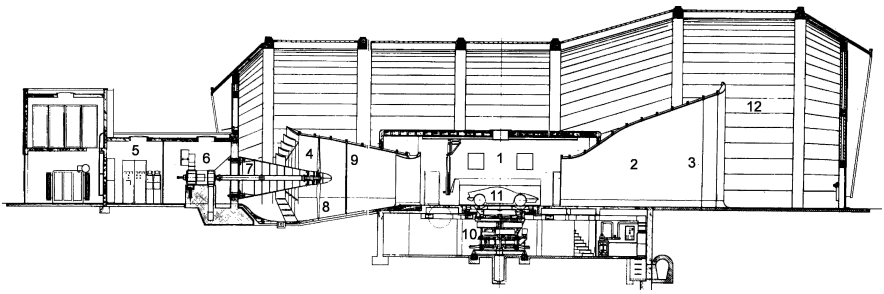

FIGURE 21.39. Schematic cross-section of the Pininfarina wind tunnel. 1) test chamber; 2) intake cone; 3) turbulence generators; 4) outlet cone; 5) power conditioning units; 6) motor; 7) propeller shaft; 8) propeller; 9) nets; 10) six-component force transducer; 11) vehicle under test; 12) building.

lift would affect the measurement of aerodynamic actions. If, on the contrary, the wheels are actually in contact with the ground, they would exchange forces with the carpet, affecting again the measurement of forces and moments, unless the whole system, carpet included, is on the balance measuring the forces. In that case, the forces between wheels and carpet are internal forces and are not measured.

Alternatively, it is possible to use a narrow, moving carpet located inside the wheels, which are supported on the fixed floor (hence rotation of the wheels is not simulated) or on rollers. In whatever way the motion of the ground is simulated, the problem of the boundary layer on the ground remains. As shown in Fig. 21.40a, if the ground does not move with respect to the vehicle, the latter is partially in the boundary layer of the ground.

The simplest way to simulate the presence of the ground is to use a second vehicle located in a mirror position with respect to the ground that physically does not exist (Fig. 21.40b). This approach is difficult to apply in full size testing, since the two vehicles must be suspended in a way that does not disturb the aerodynamic field, and the cross section of the jet is doubled. It is much easier to apply it in tests on models.

The approaches shown in Fig. 21.40c, d, g, h, i are based on aspiration, or blowing the boundary layer so that the velocity profile of the air close to the ground is similar to that occurring when the vehicle moves with respect to it. In Fig. 21.40e, f the vehicle is at a distance from the floor, on a surface (that does not move) simulating the ground, or on nothing. In the latter case, the wheels are in a different situation from the actual one. In Fig. 21.40l a small deflector deviates the air stream to the sides, to reduce the boundary layer of the ground.

In Fig. 21.40m, n, o, three ways to allow the rotation of the wheels are shown. One large roller, two small rollers or a belt supported by three rollers allow the wheels to rotate. They must be located on the balance, so that the forces they exchange with the vehicle are not measured along with the aerodynamic forces. An alternative is to substitute soft elements, similar to brushes, for the ground

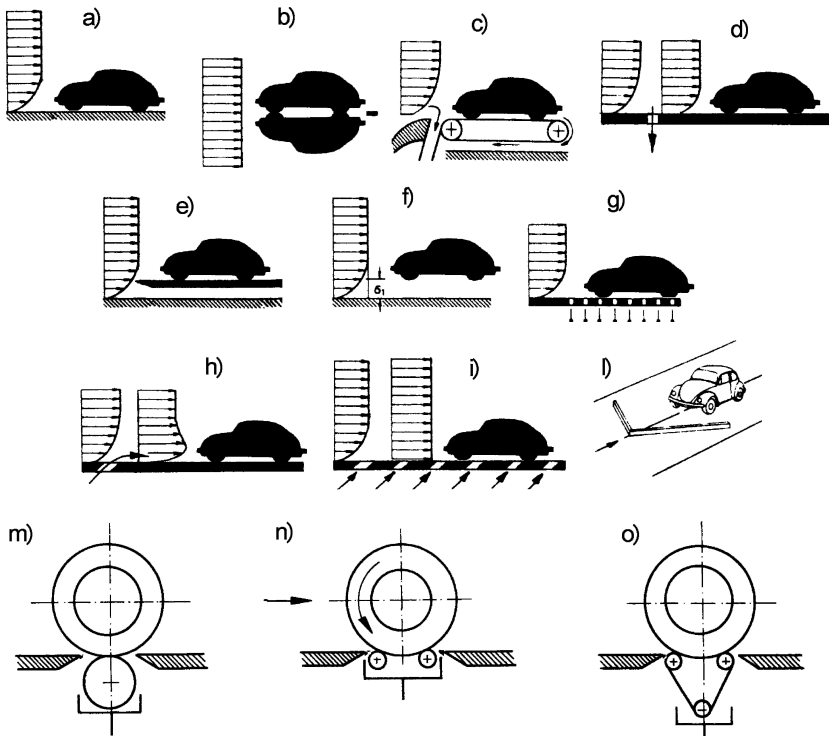

FIGURE 21.40. Simulation of the moving ground (a-l) and rotating wheels (m-o) in wind tunnel testing.

under the wheels, allowing them to rotate but blocking the air flow beneath them and producing no large forces that may affect measurements.

Another problem is that of air turbulence. Aeronautic wind tunnels are usually designed to have the lowest possible turbulence, while the air vehicles meet as they move, particularly on windy days, is more or less turbulent. Nets or other devices to increase air turbulence are therefore used in automotive wind tunnels.

Automotive aerodynamics is based on full scale tests, as we have seen; however, tests on reduced scale models are also used, especially for industrial vehicles or in the early development stages of cars. The main advantage of tests on models is their reduced cost, both in the construction and modifying of models and the use of small size tunnels. Nor is the cost reduction due to the reduced time needed to prepare and perform tests negligible. The disadvantages of models are linked to their limited geometric similitude and to the difficulty of obtaining a good dynamic similitude. Both these problems increase when model sizes are reduced.

In 1/2 or 1/3 scale models it is possible to reproduce tiny details (to study internal flows, internal details of the engine compartment must also be reproduced),

even if this causes an increase in the cost of the models. It is difficult to maintain detailed geometrical similarity if the scale is smaller.

To achieve dynamic similarity, the Reynolds number must be the same as in the actual vehicle, and the simplest method is to operate at a correspondingly increased speed. Again, this is possible in tests at 1/2 or 1/3 scale, while for models in smaller scale the required speed may be too high, with a correspondingly high Mach number, that may lead to erroneous values for the aerodynamic coefficients.

While in aeronautic closed circuit tunnels it is possible to operate at a pressure higher than atmospheric pressure (by increasing the pressure the kinematic viscosity decreases and the Reynolds number increases), open circuit tunnels must operate at atmospheric pressure and thus cannot compensate for the small scale of the model.

In spite of all the above problems, wind tunnel tests, particularly if performed on full scale vehicles with simulation of internal flows, remain the best way to measure aerodynamic forces and moments acting on road vehicles.

For the measurement of drag alone, it is possible to perform road tests in which the vehicle is allowed to coast down from various speeds on level road: From the deceleration law the total drag acting on the vehicle is computed. The main drawback of these tests is that it is impossible to separate the contribution of drag due to aerodynamics from that due to rolling resistance and all other forms of drag caused by the mechanical elements operating during the test. If rolling resistance were independent from the speed and C_x were constant, function dV/dt would be of the type:

$$\frac{dV}{dt} = \left(-f_0 mg - \frac{1}{2}\rho S C_x V^2 \right) \frac{1}{m_{at}} , \tag{21.23}$$

and hence it would be enough to approximate the measured law dV/dt with a parabola and to compute C_x from the coefficient of the quadratic term.

The actual rolling resistance is of the type

$$F_r = -mg(f_0 + KV^2) ,$$

and both forms of drag are included in the quadratic term. Only using experimental data on rolling resistance in operating conditions is it possible to interpret coast-down tests correctly. It is possible to obtain realistic values of the aerodynamic drag, and hence of C_x, if tests of the type of those shown in Fig. 2.75 are performed on the whole vehicle.

Even if the aerodynamic field cannot achieve the correct configuration characterizing the steady state conditions at any speed during a cost down test, these tests are usually performed to compare the values of C_x obtained in the wind tunnel with those obtained in close to actual operating conditions, although the latter may be approximated,.

21.7 NUMERICAL AERODYNAMICS

In the last thirty years, numerical methods based on various discretization techniques applied to the Navier-Stokes equations were developed. The diffusion of such methods, usually referred to as numerical or computational aerodynamics, has been made possible by the availability of computers with increasing power and by the introduction of new computational techniques.

While in aeronautics computational aerodynamics has reached a point where it is possible to compute in a precise and reliable way the aerodynamic field and forces acting on aircraft (even if the validation of the results with experimental tests in the wind tunnel are still needed), in road vehicle aerodynamics the possibility of using computational aerodynamics to substitute at least partially for wind tunnel testing remains controversial, and we seem to be still far from achieving this goal.

This difference is linked with the difficulty of predicting numerically where the flow detaches from the body: computational aerodynamics yields very good results in case of attached flows, but when large wakes or separation bubbles are present the computation becomes more difficult and the results less reliable. Numerical methods may, on the contrary, be used without problems in automotive aerodynamics if the location where the flow detaches is known.

Numerical aerodynamics is based mainly on the discretization of the aerodynamic field, and on the use of a simplified form of the Navier-Stokes equations. The simplest approach is the use of the boundary elements method, which in aerodynamics is often referred to as the panels method. Only the surface of the body needs to be discretized (Fig. 21.41a). This is a linearized method, and can be used on an attached inviscid flow, although it may be applied also to zones where the separation zone is known and described geometrically with high precision. It is a technique widely used in aeronautics, but in the automotive case it requires the use of experimental techniques to define the zones where the flow separates.

The methods based on the discretization of the whole aerodynamic field up to a certain distance from the vehicle (finite differences method, finite elements method (FEM, Fig. 21.41b)) allow nonlinear forms of the Navier-Stokes equations to be discretized as well, and the zone where the flow detaches to be computed through iterative techniques. Combined approaches are also possible, to combine the advantages of the various methods.

An example of the computation of the pressure distribution, accurately obtained using the finite volumes methods, is shown in Fig. 21.42[17]. To obtain such a good result, the aerodynamic field was subdivided into more than 5 million cells.

---

[17]H. Wustenberg, B. Huppertz, reported in S.R. Ahmed, *Computational Fluid Dynamics*, in W.H. Hucho (Ed.), *Aerodynamics of Road Vehicles*, SAE, Warrendale, 1998.

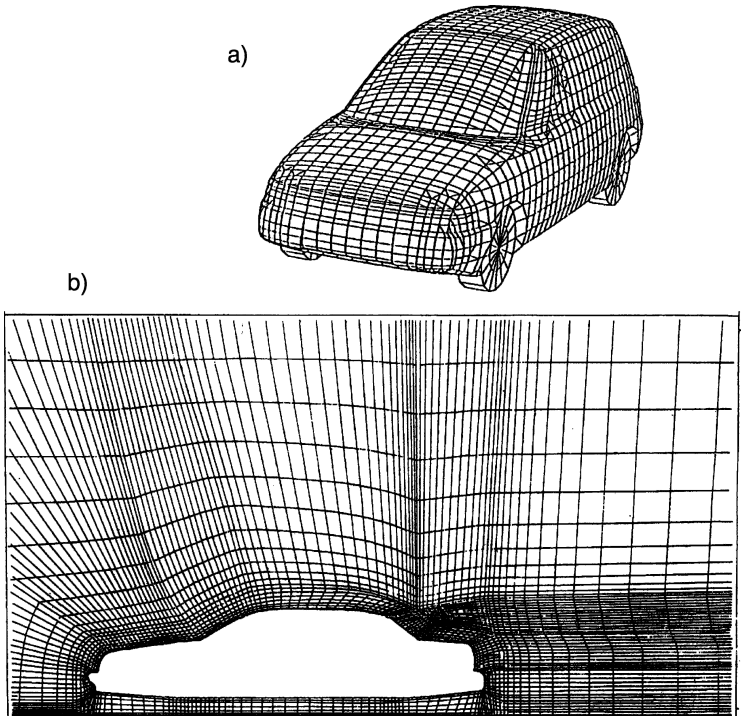

FIGURE 21.41. Discretization of the surface of a car to compute the aerodynamic field using the panels method (a) and of the whole aerodynamic field using the finite element approach (b).

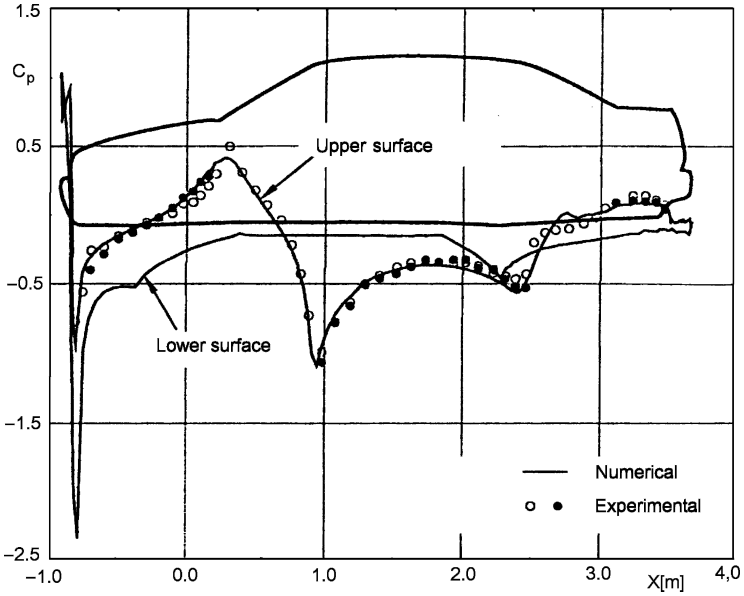

FIGURE 21.42. Pressure distribution in the symmetry plane computed using the finite volumes method.

The hopes that numerical aerodynamics raised must be at least partly downsized, even if it is becoming (or better, may become in the future) a powerful tool. It allows the aerodynamic behavior of the vehicle to be studied with a reduced number of wind tunnel tests, simultaneously increasing the number of configurations studied and helping in the interpretation of the experimental results. However, it is not certain that it my become, in the foreseeable future, an alternative to experimental testing.